MASTER

Intelligent charge controller design for off-grid solar street lighting

Haider, S.

Award date:
2014

Intelligent Charge Controller Design for Off-Grid Solar Street Lighting

SHAYAN HAIDER

SUPERVISORS: DR.IR.MARC GEILEN (TU/E)

PIERRE PEETERS (PHILIPS LIGHTING)

PREFACE

The thesis work has been carried out at Koninklijke Philips N.V. with the intent to shift the existing generation solar off-grid outdoor lighting solutions to a higher density Lithium-ion battery technology and improve its power efficiency. I would like to acknowledge all the people and institutions that have contributed directly and indirectly in this work.

First of all, thanks to the God Almighty for all his blessings that enabled me to complete this thesis project.

I would like to thank my company supervisors, Dr. Eliav Haskal (Philips Research) and Pierre Peeters (Philips Lighting), for their assistance, support and dedication to this project. I am especially thankful to Pierre Peeters for countless stimulating, inspiring technical discussions. Besides the relationship from a student to supervisor, I always felt a good level of friendship and cooperation. I am also grateful for the guidance given by Trung Thanh Nguyen (Philips Research).

I would also like to thank my university supervisor Dr. Marc Geilen for his constant support and valuable feedback throughout this work.

I would like to dedicate this work to my parents for their unconditional support and love throughout my life and without whom prayers I wouldn't have succeeded this far in my life.

Last but not the least I would like to thank my friends for giving me the necessary impetus regarding the development of this thesis project, and specially my fiancée Atefeh for her comprehension, encouragement and collaboration.

Table of Contents

1. INTRODUCTION

With the limited fossil fuel reserves rapidly depleting, it is feared that the world will soon run out of its energy resources. For developing countries whose economy heavily relies on the use of such energy resources, this is a matter of grave concern. It is highly desirable that renewable energy resources with maximum conversion efficiency should be utilized in order to cope with the ever increasing energy demand. Furthermore, the global economic and political conditions that tend to make countries more dependent on their own energy resources have caused growing interest in the development and use of renewable energy based technologies [1]. Similarly, global warming and green energy policies have been a hot topic on the international agenda in the last years. Countries around the world are trying to reduce their greenhouse gas emissions. For example, the EU has committed to reduce the emissions of greenhouse gas to at least 20% below 1990 levels and to produce no less than 20% of its energy consumption from renewable sources by 2020 [2].

Street lighting systems around the world consume around 43.9 billion kilowatt-hours (kWh) every year, besides 1900 million tons of CO_2 is produced in electricity generation in order meet to this demand. Due to these aspects, street lighting has been identified as a demanding application in need of an upgrade to renewable technology. Solar photovoltaic technology in one of the first among several renewable energy technologies adopted worldwide for meeting the basic needs of solar lighting systems particularly in remote off-grid areas. However, there is a major drawback to solar power as energy can only be produced when the sun is shining. To overcome this, usually solar panels are coupled with back up rechargeable batteries, which can store the power generated during the day and use it to provide energy to systems when during the night when there is no sun shining. The toughest challenge for these systems is to provide reliable long-term service to the equipment they support. This project aims at designing a prototype intelligent charge controller to validate a newer high density Lithium-ion battery approach in challenging solar-powered off-grid lighting.

1.1 OFF-GRID SOLAR LIGHTING IMPERITIVE [3]

Approximately 1.6 billion people in the world live off-grid without electricity. This has profound ramifications. After sunset, the people living in these remote areas have either no or a very limited light access by using unsafe light sources like kerosene lanterns or candles. Lack of

reliable lighting brings communities to a halt once darkness falls, affecting education, productivity and sense of security. It also hinders the ability to carry out basic activities at night or in the early morning degrading the general quality of life. Due to the slow growth of electrification in under developed countries, the global lighting crisis increasingly separates those with access to reliable lighting from those who lack it. This leaves a substantial proportion of the world's population further behind with Africa accounting for a major share of the un-electrified of approximately 110 million off-grid households encompassing 580 million individuals.

- **Impact on the Environment:** The cumulative effect of 1.6 billion people using kerosene and contributes heavily to global carbon emissions. In addition to the direct impacts, black carbon that is formed as a result of incomplete combustion of fossil fuels plays a strong role in accelerated warming of the lower atmosphere and melting of glacial regions.

- **Impact on Health:** Fossil fuel based lighting sources offer two-fold health implications; chronic illness as a result from inhalation of indoor air polluted with poisonous gases and risk of injury due to the flammable nature of the fuel. In India alone, 2.5 million people suffer severe burns due to overturned kerosene lamps annually.

- **Impact on income generating activity:** Several studies conducted in the developing countries show that access to a lighting source of high enough illumination has significant positive impact on productivity levels and income-generating activities. For many rural households, it can be a quiet time consuming task to travel long distances in order to obtain fuel for lighting purposes. Since such activities are often undertaken by women and children, it reprieves the children from receiving essential education and limits the time available to women for income-generating activities.

1.2 PROJECT SCOPE

Figure 1.1 shows main components of an off-grid solar-powered street or area lighting system. It consists of a PV panel which converts sunlight into electric power, a charge controller which regulates battery charging and operation of the luminaire, energy storage in the form of secondary batteries and a luminaire. The main function of a charge controller is to regulate the voltage and current from PV solar panels into a rechargeable battery. It disconnects the PV panel when the battery is fully charged and keeps the battery fully charged without damage. It also protects the battery from overcharging and excessive discharging. The goal of this thesis is to design an

intelligent charge controller prototype capable of effectively charging lithium-ion batteries.
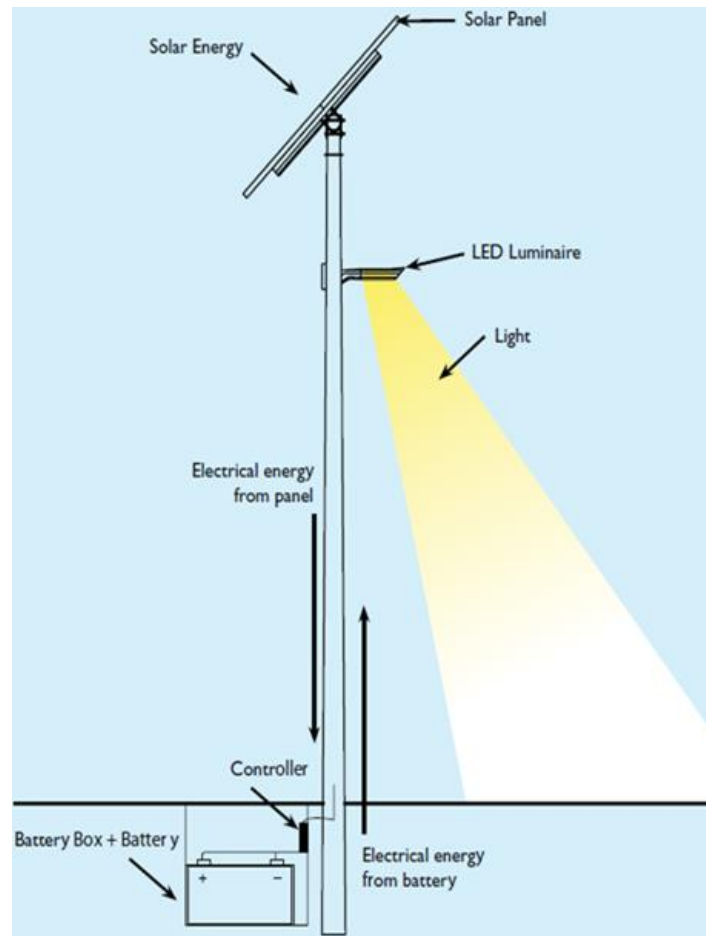
Figure 1.2: Main Components within an off-grid solar lighting system

1.3 PROJECT MOTIVATION

Photovoltaic system offers the benefits of clean non-polluting energy generation with very little maintenance requirement and a very long lifetime. Due to these advantages, today, the photovoltaic is one of the fastest growing markets in the world. However, PV power is still considered to be expensive, and the cost reduction of an off-grid solar-powered lighting system is subject to extensive research.

From the electronics point of view, this goal can be approached by maximizing the energy output of a given PV panel and prolonging cycle life of the rechargeable battery. By doing so, the size of PV panel and battery can be reduced which minimizes the total cost of a solar powered lighting system. Improving the efficiency of the PV panel and power converter is not easy as it depends on

the technology available, it may require better components, which can increase system cost. Instead, improving the tracking of the maximum power point (MPP) of the PV panel and battery lifetime extension new intelligent algorithms is easier. The DC/DC converter should ensure the highest possible conversion efficiency, while the maximum power point tracking (MPPT) control should operate the PV array at the optimum working point (MPP) in all environmental conditions. With a considerable amount of PV capacity today is installed in temperate climate zones, where passing clouds are often present (varying irradiation conditions), insuring optimal operating conditions is also becoming more crucial.

1.4 PROJECT OBJECTIVES

In accordance with the need to maximize the energy output of PV panel and prolong battery life, the project has three main objectives:

- to develop a highly efficient MPPT algorithm that is suitable for fast changing environmental conditions.
- to develop a novel control technique that maximizes DC/DC power conversion efficiency under all operating conditions.
- to develop new strategies to prolong battery life and maximize its run-time.

1.5 MAIN CONTRIBUTIONS

The main contributions of this thesis can be summarized as follows:

In Chapter 2 an improved MPPT algorithm, new ideas for overcoming the challenges associated with rapidly changing irradiation levels and the effect of partial shading, is presented, based on the well-known perturb and observe (P&O) method. The proposed algorithm enhances the steady-state and dynamic responses by introducing a variable step-size and the issue with partial shading conditions is addressed with periodic global scans.

In Chapter 3 a novel control technique for maintaining higher power conversion efficiency in low lighting conditions, is presented. The technique also helps in extending the effective charging duration.

In Chapter 4, a run-time extension algorithm is presented that maximizes battery run-time by dynamically adjusting the load profile based of the weather data so the system is able to survive a number of dark days. This technique helps in reducing the battery size by 30%.

1.6 THESIS ORGANIZATION

The thesis is organized in an order such as to provide the readers with a general understanding of the different components present in the photovoltaic battery charging system.

Chapter 2: presents an overview of the photovoltaic technology and most popular MPPT methods, analyzing their advantages and disadvantages. Problem with MPP tracking in fast-changing irradiation and partial shading is discussed. Furthermore, a P&O based MPPT method, suitable for rapidly-changing environmental conditions, is presented and analyzed.

Chapter 3: presents an overview of the commonly used DC/DC converter topologies. Modes of operation for different topologies are analyzed with the principle of inductor volt second balance. The proposed converter topology used in this project is discussed. Furthermore, a new control technique, suitable for maintaining high power conversion efficiencies in low lighting conditions is proposed, and it implementation details are presented following the experimental results.

Chapter 4: presents an overview of the Lithium-ion battery technology and its related safety concerns. Different Li-ion charging methods are discussed and a flexible charging approach in proposed. Furthermore, the chapter presents a run-time extension algorithm that adopts the load profile based of the weather data to maximize run-time.

Chapter 5: presents the implementation details of the prototype charge controller design. The experimental results collected during the limited field trial of the prototype charge controller are presented in this chapter.

Chapter 6: summarizes the work which has been carried out in this project. The chapter ends with an outlook to further research which has been enabled by the work presented in this thesis.

2. PHOTOVOLTAIC SUBSYSTEM

2.1 PHOTOVOLTAIC THEORY

Solar cells operate on the basis of the photoelectric effect (Figure 2.1). The effect occurs when photons within the electromagnetic radiation produced by the sun strike a semiconductor material. Maini and Agrawal (2007) explain that these photons can reflect off the surface of the semiconductor material, pass through the semiconductor material without striking anything, or be absorbed by electrons in the semiconductor material's crystal lattice. Once these photons are absorbed and excite the electrons in the material's crystal lattice, the electrons which are tightly bound in covalent bonds between atoms are able to move freely throughout the material. The electrons leave behind an electron 'hole' which can then be filled by another electron of a nearby atom creating another electron 'hole' hence allowing the flow of electric current.
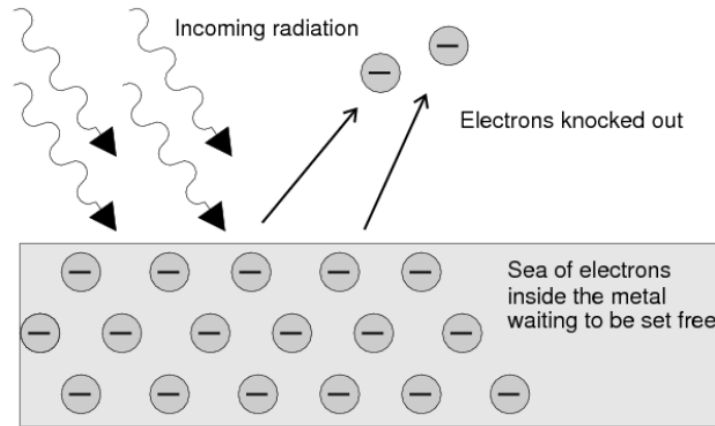
Figure 2.1: Photoelectric effect (Horner, 2011)

2.2 PHOTOVOLTAIC CELL MODEL [4]

Numerous equivalent circuit representations are available in the literature that tries to characterize the behavior of photovoltaic cells, shown in Fig. 2.2.1. Most of the equivalent circuits are variations of the basic model called the single diode model [4]. One version of the single diode model is shown in Fig. 2.2.2 and can be described by (2.1), where I_{ph} is the current generated by the incoming light, I_O is the diode reverse saturation current, n is the diode ideality factor, V_{th} is the thermal voltage, R_s is the series resistance and G_p is the shunt conductance [5].

$$I = I_0 \left[\exp\left(\frac{V - IR_s}{nV_{th}}\right) - 1 \right] + (V - IR_s)G_p - I_{ph} \qquad (2.1)$$

The thermal voltage is defined as $V_{th} = \frac{kT}{q}$, where k is the Boltzmann constant, T is the temperature in degrees Kelvin and q is the elementary charge.
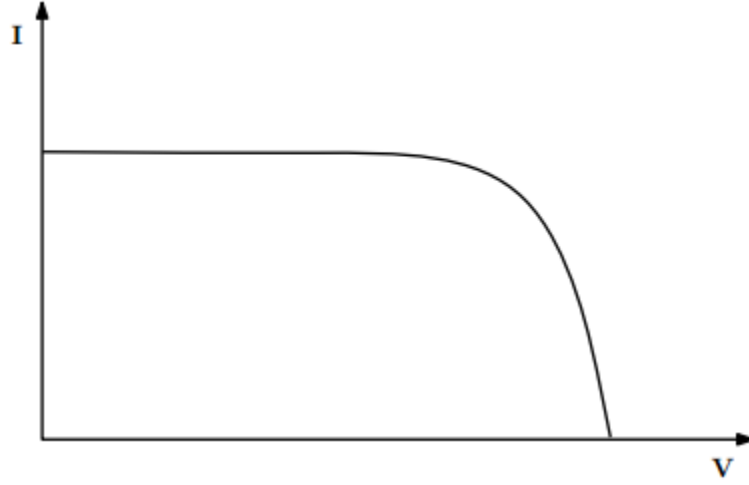
Figure 2.2.1: Typical Current-Voltage curve for a photovoltaic cell
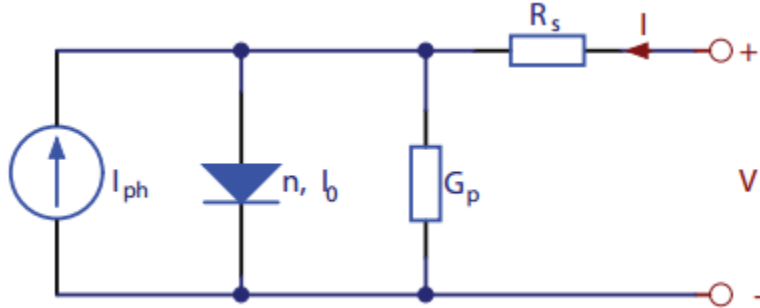
Figure 2.2.2: Typical Current-Voltage curve for a photovoltaic cell [5]

2.3 OPEN CIRCUIT VOLTAGE, SHORT CIRCUIT CURRENT AND MAXIMUM POWER POINT

There are two important points of the current-voltage characteristic curve of the PV panel; the open circuit voltage V_{OC} and the short circuit current I_{SC}. At both of these points, the power generated is zero (see Figure 2.3). V_{OC} can be approximated from (2.1) when the output current of the cell is zero, i.e. $I = 0$ and the shunt resistance R_s is neglected. It is represented by equation (2.2). The short circuit current I_{SC} is the current at $V = 0$ and is approximately equal to the photo generated current I_{ph} as shown in equation (2.3).

$$V_{oc} \approx \frac{AkT}{q} \ln\left(\frac{I_{ph}}{I_O} + 1\right) \qquad (2.2)$$

$$I_{SC} \approx I_{ph} \qquad (2.3)$$

The maximum power is generated by the solar cell at a point of the current-voltage curve where

the product $V * I$ is highest. This point is known as the MPP and is unique, as can be seen in Figure 2.3.

Figure 2.3: Important points in the characteristic curves of a solar panel

2.4 TEMPERATURE AND IRRADIANCE EFFECTS
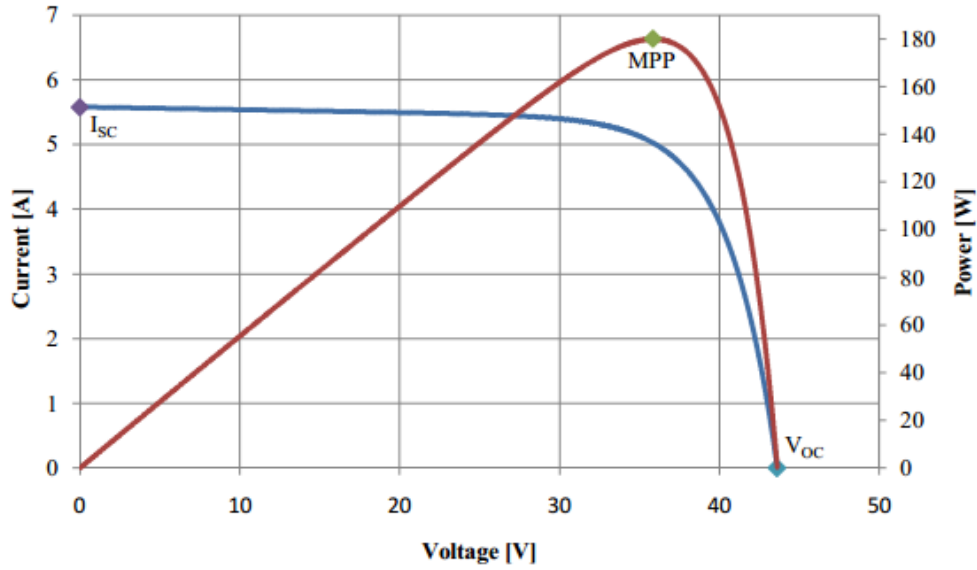
The two important factors that strongly affect the characteristic behavior of PV panel are the irradiation and the temperature. As a result, the MPP varies during the course of a day and which is the main reason why the MPP must be constantly tracked to ensure that the maximum available power is obtained from the panel.

The effect of the irradiance on the voltage-current (V-I) and voltage-power (V-P) characteristics is depicted in Figures 2.4.1 and 2.4.2 respectively. The photo-generated current I_{ph} is directly proportional to the irradiance level, so an increase in the irradiation level leads to a higher photo-generated current. Similarly, the short circuit current is directly proportional to the photo-generated current. When the operating point is not the short circuit, at which no power is generated, the photo-generated current is the main factor in the PV current, as expressed by equations (2.1). Because of this dependence, voltage-current characteristic varies with the irradiation. On the other hand, the effect in the open circuit voltage is relatively small, as the dependence of the photo-generated current is logarithmic, as can be seen in equation (2.3).

It can be seen that change in the current output in relation to irradiation is greater than in the respective change in voltage level. In practice, the voltage dependency on the irradiation is often
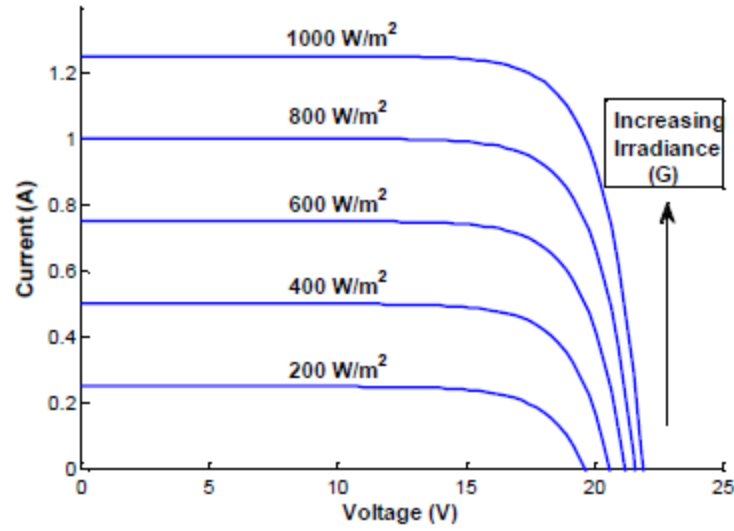
Figure 2.4.1: I-V curve with different irradiance
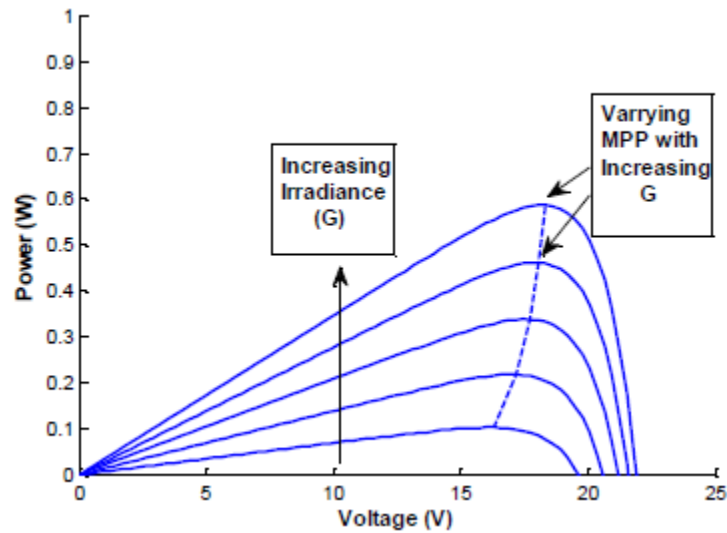
Figure 2.4.2: P-V curve with different irradiance

neglected [6]. As the effect on both the current and voltage is positive, i.e. both increase when the irradiation rises, the effect on the power is also positive: the more irradiation, the more power is generated.

The temperature, on the other hand, affects mostly the voltage. The open circuit voltage is linearly dependent on the temperature, as shown in the following equation:

$$V_{oc}(T) = V_{oc}^{STC} + \frac{K_{V,\%}}{100}(T-273.15) \qquad (2.4)$$

According to (2.4), the effect of the temperature on V_{OC} is negative, because K_V is negative, i.e. when the temperature rises, the voltage decreases. The current increases very slightly with the temperature does not compensate the decrease in the voltage caused by a given temperature rise. That is why the power also decreases. As the effect of the temperature on the current is really small, it is usually neglected [6]. PV panel manufacturers provide in their data sheets the temperature coefficients, which are the parameters that specify how the open circuit voltage, the short circuit current and the maximum power vary when the temperature changes. Figure 2.4.3 shows how the voltage-current and the voltage-power characteristics change with temperature.
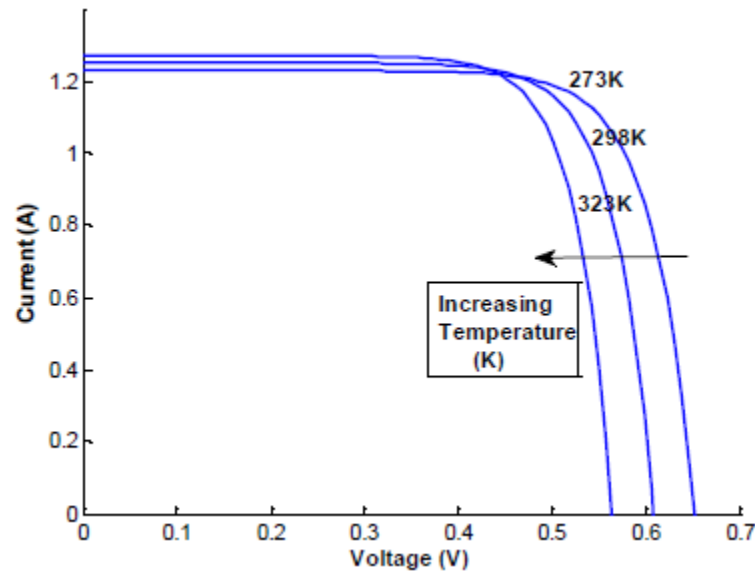
Figure 2.4.3: I-V curve for varying temperature

As previously mentioned, the temperature and irradiation depend on the atmospheric and environmental conditions, which are not constant during the year. The conditions can also change rapidly even during the course of a single day due to fast moving clouds, which causes the MPP to move constantly. If the operating point is not close to the MPP, great power losses occur as can be seen in Figure 2.3. Hence it is essential to track the MPP in any conditions to assure that at any time instance, maximum available power is obtained from the PV panel.

2.5 OVERVIEW OF MOST USED MPPT ALGORITHMS

The **Perturb and Observe** (P&O) is one of the so called 'hill-climbing' MPPT methods, which are based on the voltage-power characteristic of the PV panel that, on on the left of the MPP the variation of the power against voltage dP/dV > 0, while on the right, dP/dV < 0.
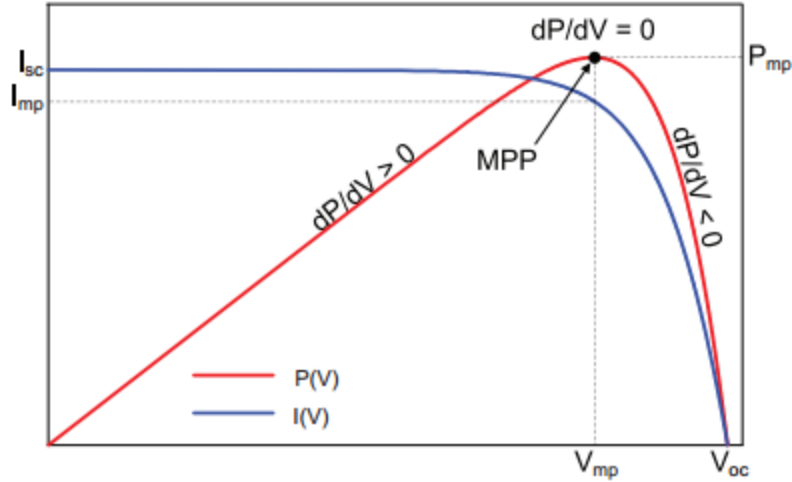
Figure 2.5.1: Sign of dP/dV at different positions on the power characteristic of a PV module [7]

It can be seen in Fig.2.5.1 that, if the operating voltage of the PV array is perturbed in a given direction and dP/dV > 0, the perturbation moved the array's operating point toward the MPP. The P&O algorithm will then continue to perturb the PV array voltage in the same direction. If dP/dV < 0, then the change in operating point has moved the PV array away from the MPP, and the P&O algorithm reverses the direction of the perturbation. Figure 2.5.2 shows the flowchart of P&O algorithm.
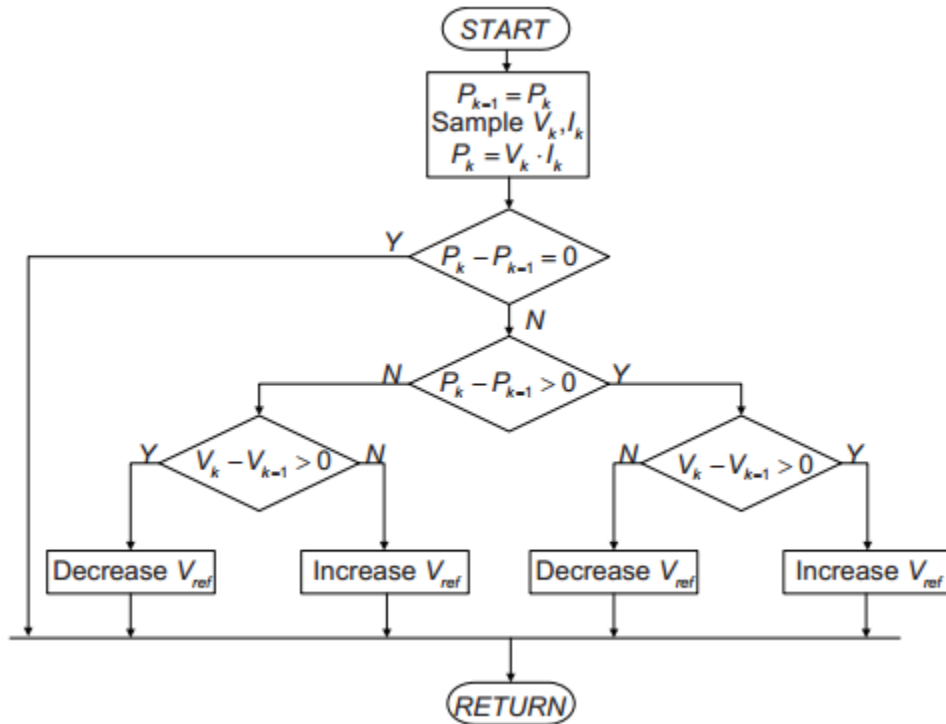
Figure 2.5.2: The flowchart of the P&O algorithm [7]

The main advantage of the P&O method is that it does not require any information about the PV array, but voltage and current measurements are needed. The simplicity of the algorithm makes it to implement with low computational demand, making P&O the most-often used MPPT method.

The two most frequently reported problems of the P&O in the literature, are the steady-state oscillations around the MPP which result in the loss of delivered power (see Figure 2.5.3), and poor tracking ability under rapidly-changing irradiations [7, 8, 9] (tracking in the wrong direction, away from the MPP). Improvement methods reported in the literature include a variable step size approach and reduction in perturbation frequency.
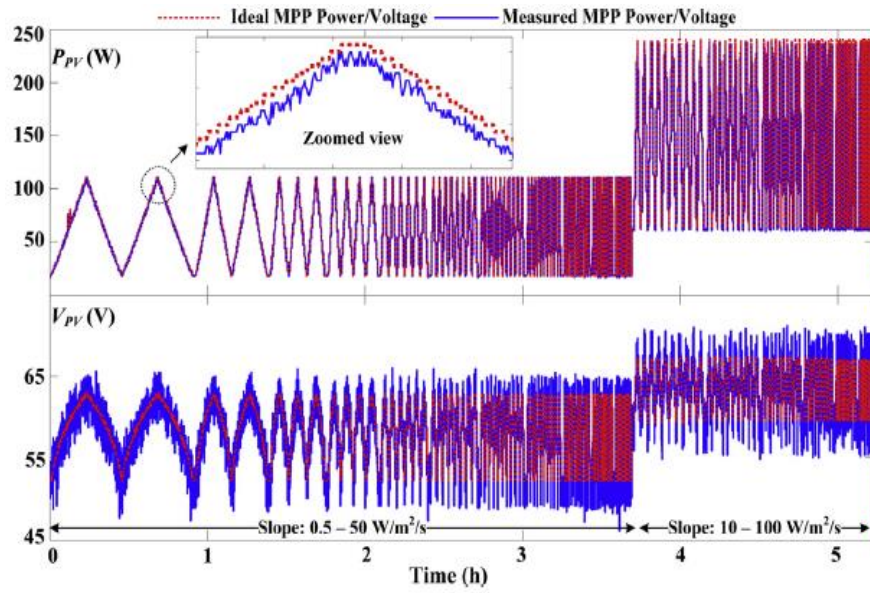
Figure 2.5.3: Delivered power loss due to oscillation around MPP

A similar hill-climbing MPPT algorithm is the **Incremental Conductance** (INC) [10], which intends to improve the P&O by replacing the derivative of the power versus voltage dP/dV used by the P&O with PV array's instantaneous (I/V) and incremental (dI/dV) conductance, according to equations (2.5) and (2.6).

$$\frac{dP}{dV} = \frac{d(VI)}{dV} = V\frac{dI}{dV} + I \tag{2.5}$$

$$\left.\frac{dP}{dV}\right|_{\substack{I=I_{mp} \\ V=V_{mp}}} = 0 \Rightarrow \left.\frac{dI}{dV}\right|_{\substack{I=I_{mp} \\ V=V_{mp}}} = -\frac{I_{mp}}{V_{mp}} \tag{2.6}$$

where,

- V_{mp} - MPP voltage
- I_{mp} - MPP current

The advantage INC offers over P&O is in its ability to find the distance to the MPP, determine when the MPP has been reached ($\frac{dI}{dV} = 0$), and hence stop the perturbation [7]. However, in practice [10] the equality in Eq. (2.2) is seldom obtained. A small marginal error has to be allowed which either limits the sensitivity of the algorithm to slight changes in environmental conditions or it will start oscillating around the MPP. Although INC method generally appears in the literature as a progress in efficiency compared to the P&O [7,8], it is not commonly used due to its implementation complexity. INC is also unable to track in the correct direction during rapidly-changing irradiations [11].

Another well-known MPPT method is the **Constant Voltage** (CV), which makes use of the relation that the PV array MPP voltage changes only slightly with irradiation. In this algorithm, the MPPT momentarily sets the PV array current to zero to allow the measurement of the open-circuit voltage. The operating voltage is set to a fixed percentage of the open-circuit voltage [7]. Although the ratio between the open-circuit voltage and MPP voltage (V_{oc}/V_{mp}) depends on the solar array parameters, a commonly used value for crystalline silicone panels is 76% [7]. This operating point is maintained for a set amount of time, after which the cycle is repeated. The main problem with this algorithm is that energy is wasted while the open-circuit voltage is measured, and V_{mp} is not always at the fixed 76% of the V_{oc} [7].

Choosing the step-size in 'hill-climbing' MPPT algorithms (P&O and INC) is very critical since it can considerably affect the overall performance of the algorithm. As can be seen in Fig.2.5.4(a), a large step-size leads to a better transient response (i.e. faster tracking), but results in large power oscillations in the steady-state. On the other hand, the choice of a small step-size leads to a slower transient response but less power oscillation at the steady state (see Fig.2.5.4(b)). Consequently, the selection criterion of the step-size is contingent on the best trade-off between the transient response speed and the steady-state oscillation.

In the literature, several comparisons have been made for the MPP algorithms mentioned above. Under high irradiation conditions, P&O, INC and CV perform equally with INC producing the highest efficiency compared to the others [7, 11, 12]. On the other hand, as irradiance decreases,

the efficiency of the P&O and INC also decrease. It is shown in [12] that at irradiations below 300W/m2, INC performs very poorly, and completely fails to track the MPP below irradiation of 50W/ m2 whereas P&O is able to track below 50W/m2 [12]. The CV method is considered to be the least efficient of the three [7], but contrary to P&O and INC, as the irradiance decreases, CV shows an improvement in efficiency as the power losses due to steady-state oscillations are dominant in lower irradiation levels. Because of this characteristic, CV is often used in combination with one of the hill-climbing methods.
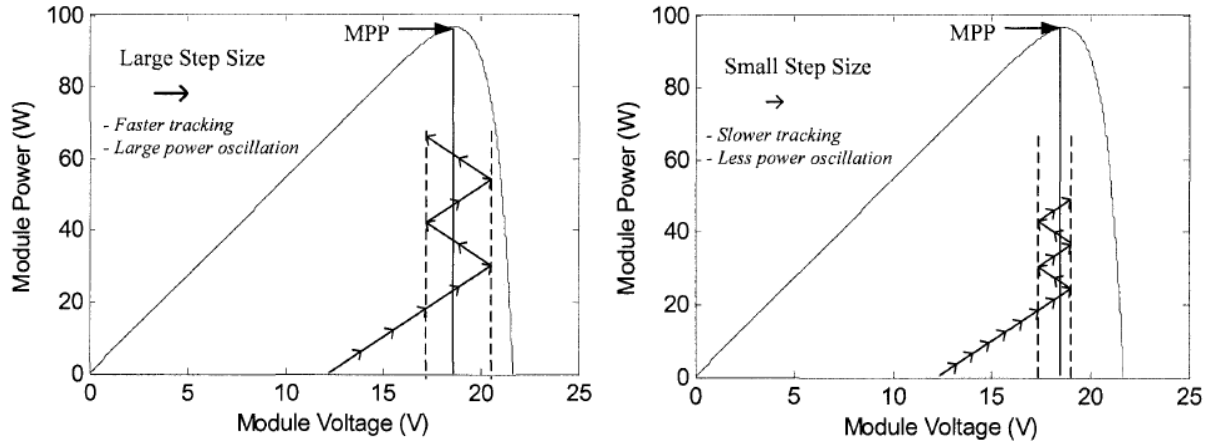
Figure 2.5.4: (a) MPPT algorithm response with a large step-size, (b) MPPT algorithm response with a small step-size

2.6 MAXIMUM POWER POINT TRACKING IN RAPIDLY CHANGING CONDITIONS [13]

P&O and INC can track in the wrong direction under rapidly changing irradiation conditions. Irradiation levels can change relatively quickly due to weather conditions, e.g. passing clouds. This changes the output from a PV panel drastically with reduced solar irradiation causing the current of the solar panel to drop.

If the change in the intensity of irradiation causes a bigger change in power than the one caused by the increment in the voltage, the MPPT can get confused, and will interpret the change in the power as an effect of its own action. This is illustrated in Figure 2.6, where;

- T_P - the perturbation period of the MPPT
- P_k, P_{k+1}- the values of power measured at the k th and the k + 1-th sampling instances
- dP - the change in power, caused by the perturbation of the MPPT
- dP_2 - the change in power, caused by the increase in irradiation
- inc - the (voltage) perturbation increment of the MPPT

Figure 2.6 [13]: In the case of slow irradiation changes, the P&O method is able to track in the right direction (a), but in case of rapidly-changing irradiation, it is unable to determine the right tracking direction (b)
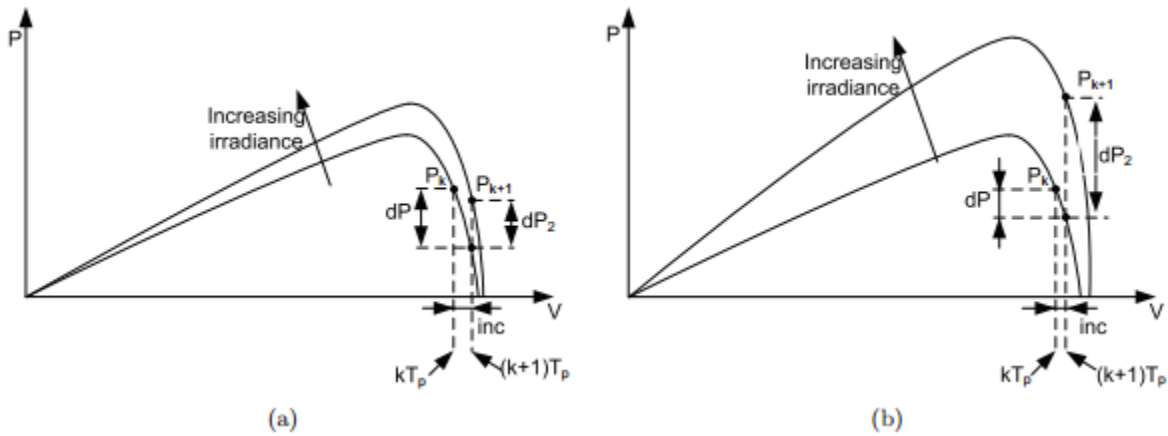
If $dP > dP_2$ the MPPT is able to interpret correctly the change in power between two sampling instances (Fig.2.6(a)), as the overall change in power will be dominated by the effect of the perturbation. On the other hand, if $dP < dP_2$, the MPPT is unable to determine the right direction of tracking as for example $P_{k+1^-} - P_{k^-}$ in Fig.2.6(b) is positive, regardless of the perturbation direction of the MPPT. In the case depicted in Fig. 2.6(a), the P&O would continue to increase the voltage reference until the irradiation change is stopped or dP becomes larger than dP_2.

2.7 PARTIAL SHADING

The voltage and power levels of a single PV cell are quite low therefore; PV cells are typically connected in series and/or parallel combination in order to deliver the required amount of power (Haberlin, 2012). Series connection of PV cells increases the maximum voltage of the system whereas and parallel connection increases the maximum current. By using both series and parallel connections, the PV system can be designed to have the desired nominal voltage and power levels.

The series connection of PV cells is, however, prone to mismatch losses if the electrical characteristics of the PV cells are not similar (Chamberlin et al., 1995) or the cells do not operate under uniform conditions due to, for example, partial shading conditions (Alonso-Garcı́a, Ruiz and Chenlo, 2006). Mismatch losses occur when all the PV cells are not operating at their own MPPs despite the fact that the whole system would operate at its own MPP. In series connection

15

the PV cell with the lowest SC current limits the current of the whole series connection (Wenham et al., 2007). Under partial shading conditions, shaded PV cells have lower SC current than the non-shaded cells. If then the current of the PV array is higher than the SC current of the shaded cell, the cell will be reverse biased with respect to the other cells in the series connection and acts as a load dissipating part of the power generated by the other cells leading to power losses.

Partial shading conditions can occur due to multiple of reasons such as buildings, trees or clouds. Shading due to static objects typically moves slowly as the Earth spins around its axis. Shading due to clouds is dynamic in a way that the shading conditions come suddenly and also leave the area of the generator quickly.

Figure 2.7 [14] shows how partially shaded conditions effect the current vs voltage graph and the power vs voltage graph of the PV array. Local maximum points can be seen clearly in the power vs voltage graph which occurs due the sudden drops in currents on the current vs voltage graph. Local maximum power points are a direct result of partial shading and are not a true representation of the MPP. The global power point is the correct maximum power point which should be tracked and maintained.
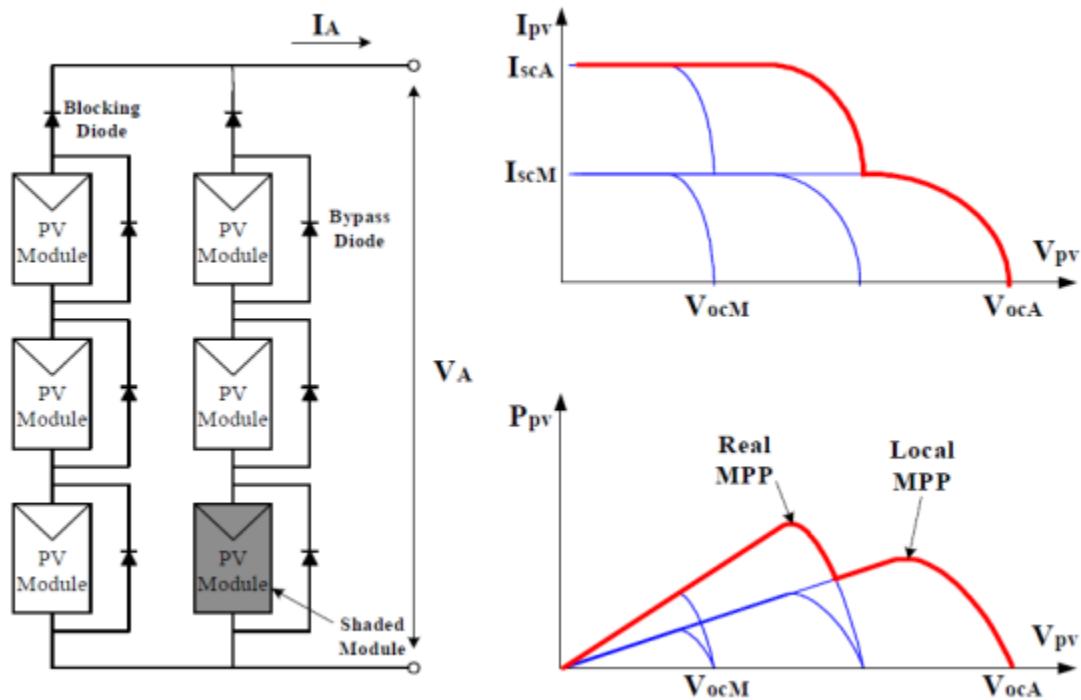

Figure 2.7: (Clockwise from left) Array with 1 shaded module, I-V output curve of array, P-V output curve of array

2.8 MPPT FAILURE IN CONTENTIONAL METHODS DUE TO PARTIAL SHADING [14]

Figure 2.8 below shows P-V and I-V graphs of a solar array under uniform irradiation, with the MPP located at point A. Under this condition, conventional MPPT schemes (INC and P&O) will be able to track the maximum power point with a higher efficiency.
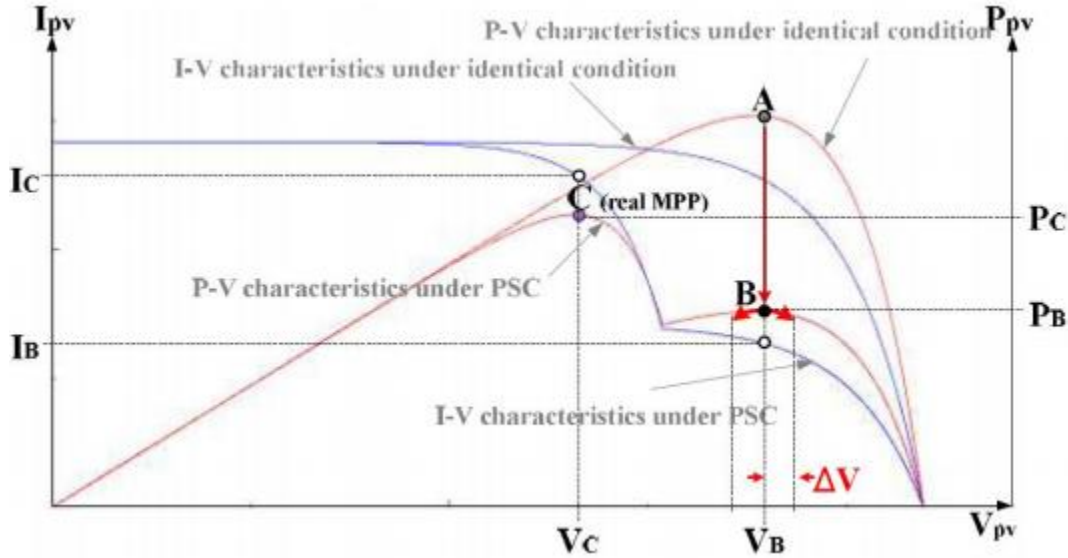

Figure 2.8: MPPT tracking failure in conventional methods [14]

However if we look at the second pair of curves under generated under PSC (Partial Shading Condition), we can see that the global maximum point of PV array has moved to C whereas a local maximum stays at B. Under this condition, the conventional MPPT algorithms will only be able to operate the PV array at B because upon reaching this point, a voltage step ΔV to the left of B will fail to move the algorithm away from this invalid maximum point as it sees the power decrease, forcing it to oscillate around this point.

2.9 PROPOSED MPPT ALGORITHM

The proposed algorithm focuses on improving tracking speed and stability, as well as overcoming the effects of partial shading and rapidly changing weather conditions. It is similar to the P&O algorithm reviewed in Section 2.5, with 2 additional elements; 1) Step-size variation (see Figure 2.9.1) , 2) Global MPP scan and Under-Voltage (UV) / Under-Current (UC) events. Step-size variation is in place to minimize energy loss through oscillations around the MPP, UV/UC events are to speed up MPPT when there is a rapid change in the levels of irradiation and global MPP scan is periodically executed to ensure the operation at the global maximum due to changing
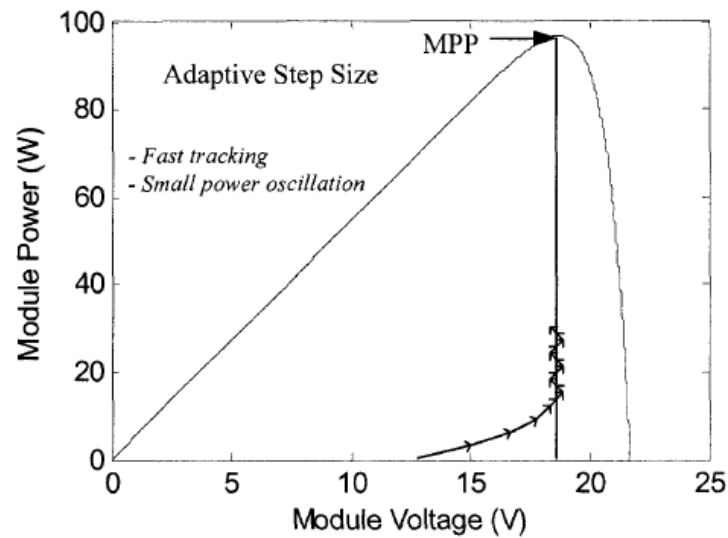
partial shading conditions.

Figure 2.9.1: Step-size variation in proposed MPPT algorithm

The algorithm employed operates from one of five states presented in Figure 2.9.2.
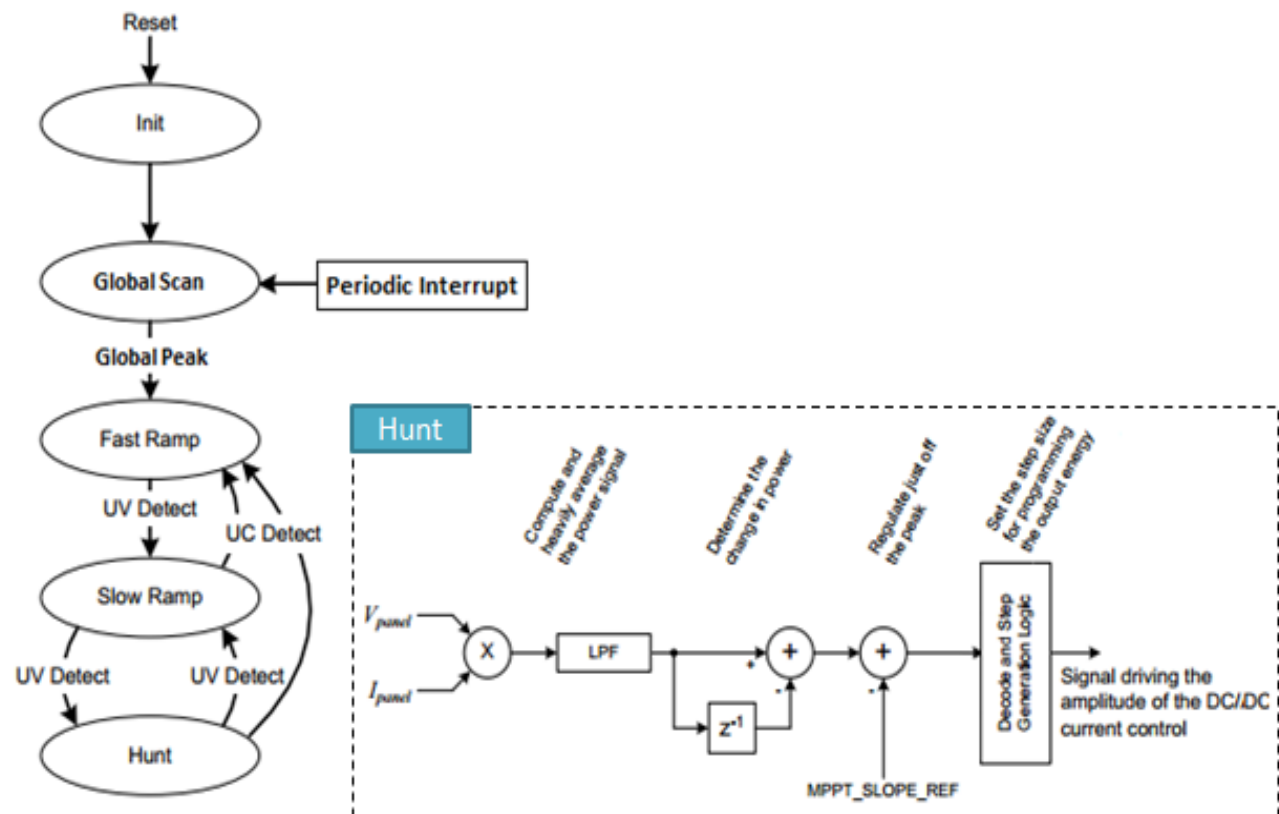

Figure 2.9.2: Proposed MPPT Operating States and Hunt Algorithm

The functionality of each state is described below;

- **Init**

    This is a temporary state in which the algorithm is completely reset for peak tracking.

- **Global Scan**

    This state consists of the I-V scan procedure and a regular P&O algorithm. It is enabled after a system reset or at periodic intervals to partially scan operating area restricted to PV voltage range (0.5 to 0.9 p.u.) under the I-V curve. The scan area is limited to reduce energy loss, since during the scanning process the operating point is away from the MPP. There is also a high probability that under majority of partial shading conditions, the global maximum is going to reside within this restricted range. Once the global maximum is found, the MPP control signal is set the new global reference and transition to the next state happens.

- **Fast and Slow Ramp**

    These states work similarly to that of the global scan. Scanning is only applied to a smaller region under the I-V curve near the global maximum. The fast and slow ramp states are functionally the same with one minor difference; the step-size. During fast ramp, large steps are taken quickly scan for the gross peak whereas in slow ramp, the step-size is significantly lower which results is a narrower find of the peak. The peak output of a panel has a major defining characteristic. If we slowly, but consistently, sweep up the current, the voltage will gradually fall based on the series losses in the panel until the knee of the power curve is hit (see Figure 2.5.1). At this point, the voltage drop is significant and measurable. The peak is found by sweeping the through the MPP control signal until a change in voltage is significant relative to the desired operating point triggering a UV event. Figure 2.9.3 shows the flowchart of procedure used to detect this change in voltage.
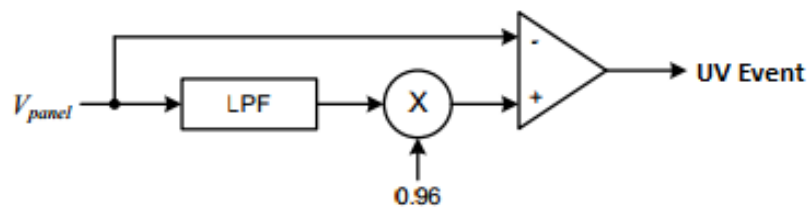

Figure 2.9.3: Proposed Voltage Change Detection

Although the peak detection algorithm is quick to find the approximate peak, it is gross in

its targeting. It will only put the control in the approximate range of the peak. The method in Figure 2.9.3 is as time-based as it is level-based because of the filter. It will improve in accuracy if the ramp is slower. Thus there are two states employed. The first is a very fast find while the second is a much slower find. The fast and slow ramp states transition to the next state by looking for a gross sudden UV transition in solar panel voltage.

- **Hunt**

   This is the final state and uses a step-size smaller than that of in slow ramp state. Figure 2.9.2 outlines the algorithm that controls hunting for the peak. The power is computed and deeply filtered to attenuate and average the power from the solar panel. This is done to compensate and slow down the natural perturbations in MPPT voltage, generated by rapid changes in irradiance that would otherwise force MPP tracking in wrong direction as explained in section 2.6. A gross change in global maximum due to change in irradiance or occurrence of partial shading will cause a significant drop in the panel current hence triggering a UC event. This event causes a transition to fast ramp stage so the new maximum point can be quickly tracked, hence increasing the sensitivity and robustness of the proposed tracking algorithm towards changes in operating conditions.

Owing to its simplicity, the proposed control method is suitable for implementation on commercially available micro-controllers. Further, it is cost-effective, as it makes use of hardware modules (A/D, interrupt service routines, etc) that come with such micro-controllers.

2.10 COMPARISON WITH CONVENTIONAL P&O ALGORITHM

To evaluate the performance of the proposed algorithm, its response is compared with three different step-size values of the conventional P&O algorithm 0.005, 0.008 and 0.01. The step-size values correspond to the threshold of MPP control signal to the power converter. In each case, the response of the P&O algorithm is presented and compared to the response of the proposed algorithm. The results are collected under a constant irradiation and temperature level, where the purpose is to verify the improvements in the transient and steady-state response of the proposed algorithm. The maximum targeted power point in the experiment conditions is at 35V, and this is set as an ideal case to calculate and compare the error in the tested algorithms.

The first comparison case is with the P&O algorithm where the step-size is set to 0.005, which is a relatively small value. The responses of the two algorithms is shown in Fig.2.10.1(a),(b); the

P&O algorithm attains the maximum power in 2.495s, as the proposed algorithm attains it in 1.265s. The error between the ideal response and that of the P&O response is calculated to be 0.252V whereas the error between the ideal output and that of the proposed algorithm response is calculated to be 0.119V. This corresponds to an improvement of 50.70% in the transient response and that of 0.38% in steady-state response. The small step-size in the P&O leads to a slow transient response but a stable steady-state response. The adaptive step-size in the proposed algorithm cannot only match the performance of the small step-size P&O, instead it leads by its fast transient response.
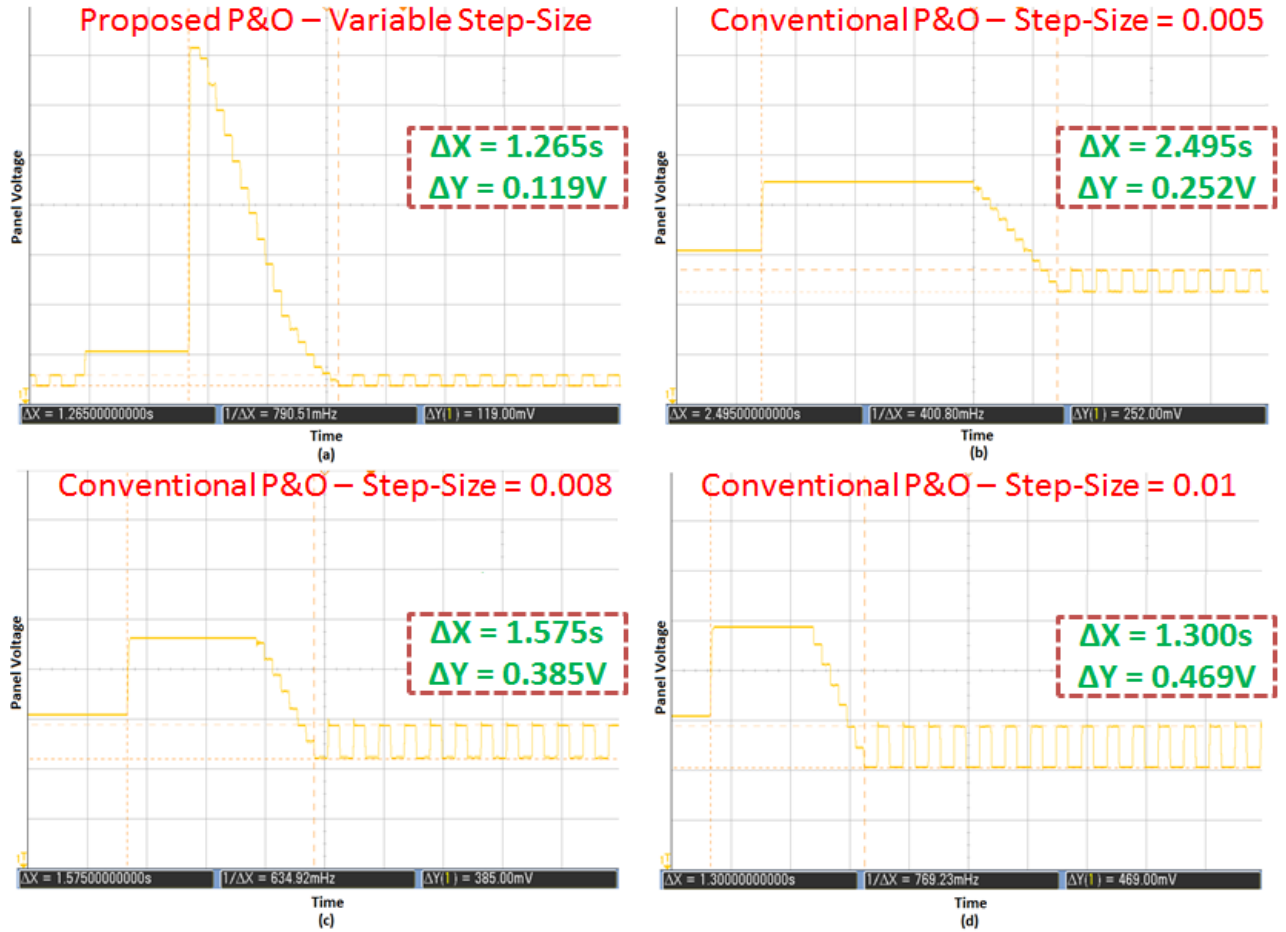
Figure 2.10.1: Comparison between the proposed algorithm and P&O algorithms with different step-sizes. (a) Proposed Algorithm, (b) Conventional P&O (Step-Size = 0.005), (c) Conventional P&O (Step-Size = 0.008), (d) Conventional P&O (Step-Size = 0.01)

For the second comparison case, a medium step-size value (0.008) is selected for the P&O algorithm. The same comparison procedure as the first case is followed, and the result is shown in Fig.2.10.1(a),(c). The conventional P&O algorithm attains maximum power in 1.575s. The error

between the ideal response and that of the P&O response is calculated to be 0.385V. This corresponds to an improvement of 19.68% in transient response and that of 0.75% in steady-state error. This larger step-size in the P&O leads to a better transient response than the first case, but small power oscillations appear in the steady-state which can cause significant power loss in the long run.

The final comparison case with the P&O algorithm is done for a large fixed step-size (0.01). The result is shown in Fig.2.10.1(a),(d), where the P&O algorithm attains the maximum power in 1.30s. The error between the ideal response and that of the P&O response is calculated to be 0.469. This corresponds to an improvement of 2.70% in transient response, with a significant improvement of 0.99% in the steady-state response which can lead to significant gain on the long run.

Conventional P&O algorithms do not consider the effect of partial shading, e.g. multiple peaks in the power function as discussed in section 2.8. Consequently, these algorithms get trapped in a local maximum (not the global maximum), and deliver a lower peak power. The proposed algorithm addresses this issue by interrupts that are executed periodically to ensure the operation at the global maximum by initiating a global scan across (see Figure 2.10.2).
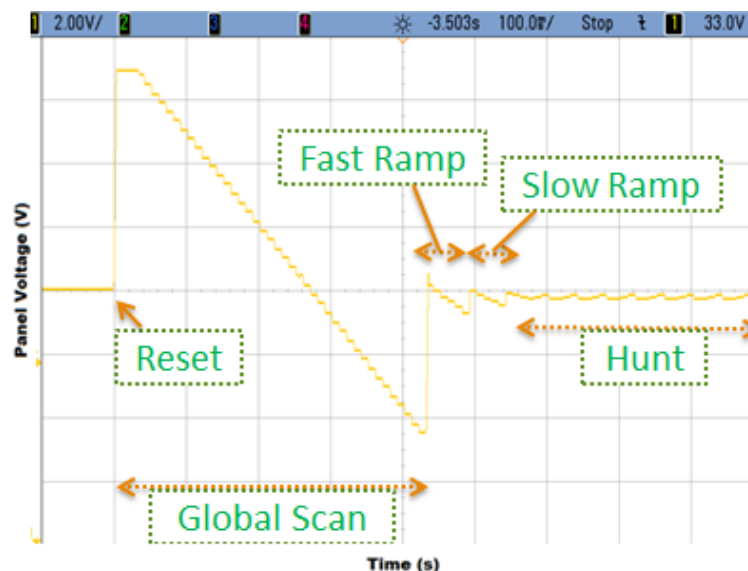
Figure 2.10.2: Periodic Global MPP Scanning

As can be seen from this comparison, the proposed algorithm shows a significant improvement over the conventional P&O algorithm (with different step-size values) and offers the least steady-

state error with faster transient characteristics.

2.11 SUMMARY

In the first part of the chapter an overview of the photovoltaic technology and most popular MPPT methods, analyzing their advantages and disadvantages is given. In the second part the problem of MPP tracking in fast-changing irradiation and partial shading is discussed. Furthermore, a P&O based MPPT method, suitable for rapidly-changing environmental conditions, is presented and analyzed.

3. POWER CONVERSION SUBSYSTEM

3.1 DC-DC CONVERTER

DC-DC power converters are employed in order to transform an unregulated DC voltage input (i.e. a voltage that possibly contains disturbances) in a regulated output voltage. For example, a DC-DC power converter can transform an unregulated (i.e. distorted) 9V input voltage in a regulated (i.e. "clean") voltage of 12V at the output. Some DC-DC power converters have a fixed output reference and ensure that such voltage is always delivered, no matter what the input is; some others can have a variable output reference, which can be therefore set depending on the current need of the device the power converter is used in.

The following section discusses various converter topologies and their operation. Idealized circuits are considered for ease of understanding and explanation. The key difference between each is the arrangement of the switch and output filter inductor and capacitor.

3.2 OVERVIEW OF COMMON DC/DC TOPOLOGIES [17]

- **Buck Converter**

The buck converter is used for step down operation. A buck converter with its output filter arrangement is as shown in Figure 3.2.1.
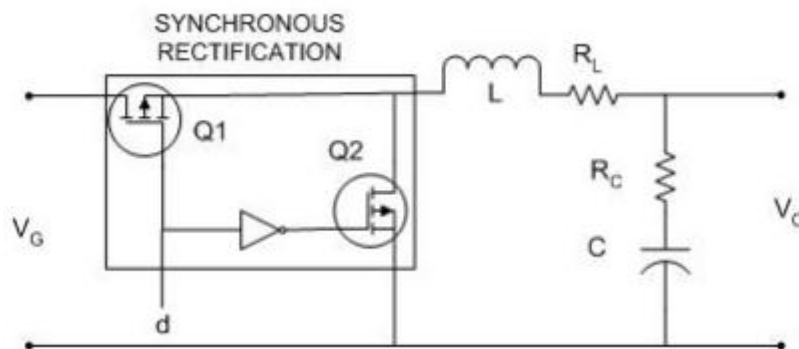
Figure 3.2.1: Buck Converter [17]

When the transistor Q1 is on and Q2 is off, the input voltage appears across the inductor and current in inductor increases linearly. In the same cycle the capacitor is charged. When the transistor Q2 is on and Q1 is off, the voltage across the inductor is reversed. However, current in the inductor cannot change instantaneously and the current starts decreasing linearly. In this cycle also the capacitor is also charged with the energy stored in the inductor. Analyzing the

inductor current waveform determines the relationship between output and input voltage in terms of duty cycle. In a well-designed converter, the main objective is to have small percentage of ripple at the output. As a result, the output voltage can be approximated by its DC component [19]. Inductor current is found by integrating the inductor voltage waveform. Inductor voltage and current waveforms for a buck converter are as shown in Figure 3.2.2.
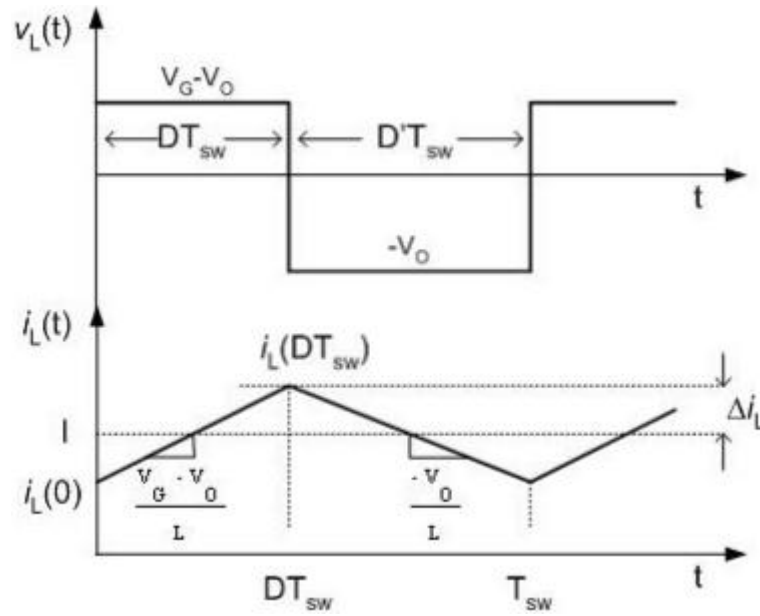
Figure 3.2.2: Steady-state inductor voltage and current waveform, buck converter [17]

In steady state, the observation that over one switching period the net change in inductor current is zero is the principle of inductor volt second balance. The inductor voltage definition is given by

$$v_L(t) = L\frac{di_L}{dt}$$

(3.1)

Integration over one complete switching period yields,

$$i_L(T_{SW}) - i_L(0) = \frac{1}{L}\int_0^{T_{SW}} v_L(t)dt$$

(3.2)

The left hand side of above equation is zero. As a result (3.2) can be written as;

$$\int_0^{T_{SW}} v_L(t)dt = 0$$

(3.3)

The equation 3.3 has the unit of volt-seconds or flux-linkages. Alternatively, total area under the vL(t) waveform over one switching period must be zero. Area under the vL(t) curve is given by,

$$A = \int_0^{T_{sw}} v_L(t)dt = (V_G - V_O)(DT_{sw}) + (-V_O)(D'T_{sw})$$
(3.4)

Average value of inductor voltage is given by,

$$\langle v_L \rangle = \frac{A}{T_{sw}} = D(V_G - V_O) + D'(-V_O)$$
(3.5)

By equating $< V_L >$ to zero and using relation d+d' = 1, and solving for V_O yields

$$V_O = D.V_G$$
(3.6)

Similar to the inductor volt-second balance, the defining equation for capacitors is

$$i_C(t) = C\frac{dv_C(t)}{dt}$$
(3.7)

Integration over one complete switching period yields,

$$v_C(T_{sw}) - v_C(0) = \frac{1}{C}\int_0^{T_{sw}} i_C(t)dt$$
(3.8)

In steady state, the net change over one switching period of the capacitor voltage must be zero, so that the left hand side of the above equation is zero. Equivalently stated the average value or the DC component of the capacitor must be zero at equilibrium.

$$\langle i_C \rangle = \frac{1}{T_{sw}}\int_0^{T_{sw}} i_C(t)dt = 0$$
(3.9)

Thus the principle of capacitor charge balance can be used to find the steady state currents in a switching converter.

- **Boost Converter**

The boost converter is capable of producing a DC output voltage greater in magnitude than the DC input voltage. The circuit topology for a boost converter is as shown in Figure 3.2.3. When the transistor is on the current in inductor L, rises linearly and at this time capacitor C, supplies the load current, and it is partially discharged. During the second interval when transistor is off,

the diode conducts and the inductor L supplies the load and, additionally recharging the capacitor C. The steady state inductor current and voltage waveform is shown in Figure 3.2.4.
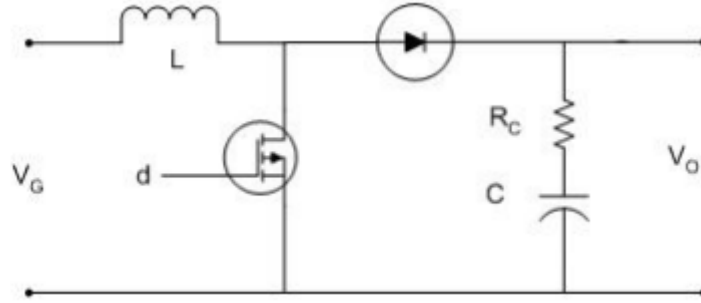

Figure 3.2.3: Boost Converter [17]

Figure 3.2.4: Steady-state inductor voltage and current waveform, boost converter [17]

Using the inductor volt balance principle to get the steady state output voltage equation yields,

$$V_G.T_{ON} + (V_G - V_O).T_{OFF} = 0 \qquad (3.10)$$

$$\frac{V_O}{V_G} = \frac{T_{SW}}{T_{OFF}} = \frac{1}{1-D} \qquad (3.11)$$

Since the converter output voltage is greater than the input voltage, the input current which is also the inductor current is greater than output current. In practice the inductor current flowing through, semiconductors, the inductor winding resistance becomes very large and with the result being that component non-idealities may lead to large power loss. As the duty cycle approaches one, the inductor current becomes very large and these component non-idealities

27

lead to large power losses. Consequently, the efficiency of the boost converter decreases rapidly at high duty cycles.

- **Buck-Boost Converter**

The buck-boost converter is capable of producing a DC output voltage which is either greater or smaller in magnitude than the dc input voltage. The arrangement for the buck-boost converter is as shown in Figure 3.2.5.
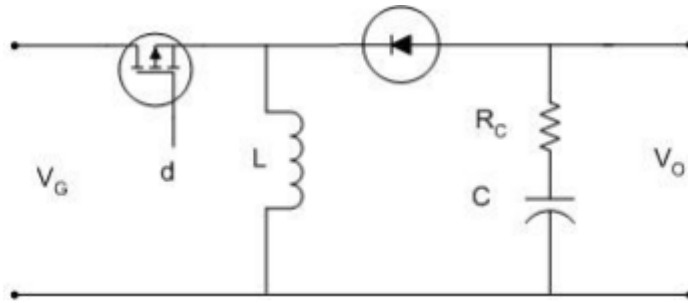
Figure 3.2.5: Buck-Boost converter [17]

When the transistor is ON, input voltage is applied across the inductor and the current in inductor L rises linearly. At this time the capacitor C, supplies the load current, and it is partially discharged. During the second interval when the transistor is off, the voltage across the inductor reverses in polarity and the diode conducts. During this interval the energy stored in the inductor supplies the load and, additionally, recharges the capacitor. The steady state inductor current and voltage waveform is shown in Figure 3.2.6.
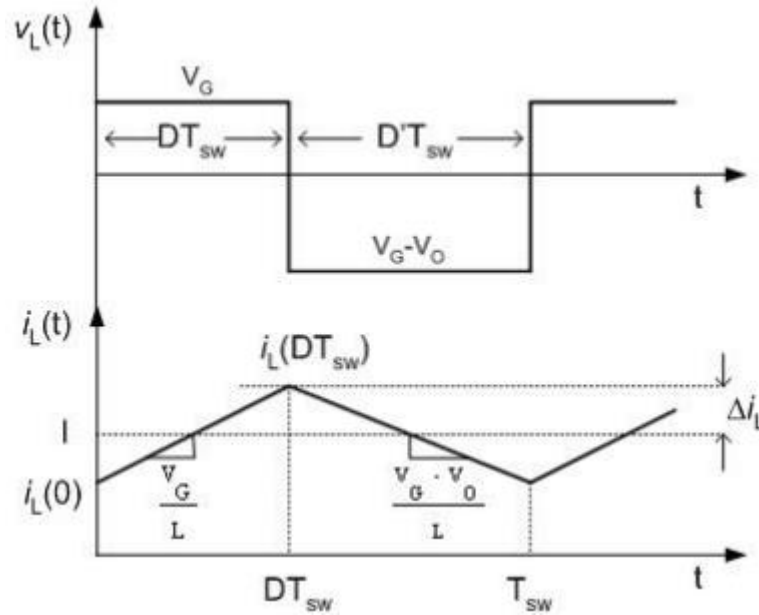

Figure 3.2.6: Steady-state inductor voltage and current waveform, buck-boost converter [17]

Using the inductor volt balance principle to find the steady state output voltage equation yields,

$$V_G \cdot T_{ON} + V_O \cdot T_{OFF} = 0 \tag{3.12}$$

$$\frac{V_O}{V_G} = \frac{T_{SW}}{T_{OFF}} = -\frac{D}{1-D} \tag{3.13}$$
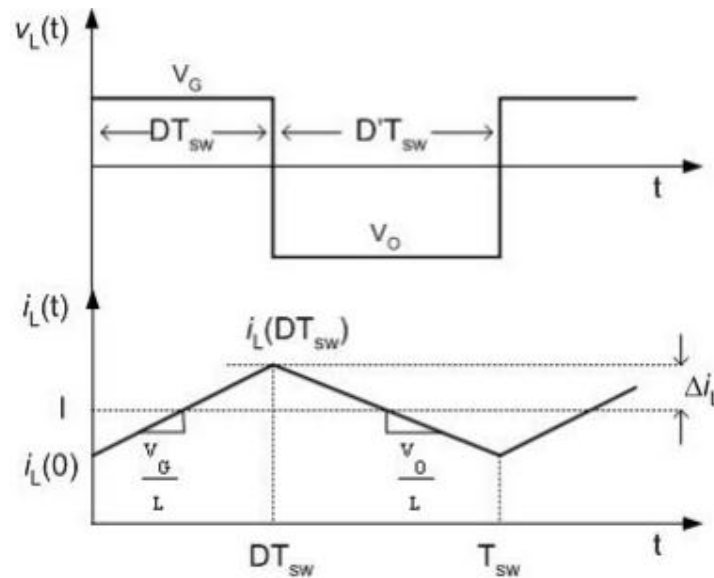
The d varies between 0 and 1 and thus output voltage can be lower or higher than the input voltage in magnitude but opposite in polarity.

- **Power Losses [18]**

There are two different types of losses occurring inside the DC/DC converter circuitry: Conduction Losses and Switching Losses.

Conduction Losses are produced because of current flowing through the following resistive media:

- MOSFETs' channel resistance RDS_{ON}
- MOSFETs' body diode
- Capacitance's ESR (Equivalent Series Resistance)
- Inductance's ESR

Being these losses of resistive type, they can be modeled to be proportional to the square of the RMS value of the current flowing inside the circuit, i.e.:

$$P_{Conduction} \sim i_{L,rms}^2 \tag{3.14}$$

This estimation is approximation, since higher losses will usually cause a rise of temperature, which is going to affect the values of the parasitive resistances, which in turn is going to affect the losses.

Switching Losses are more complicated than the previous ones. They are produced by the action of turning on and off active devices on the power's path, therefore they only happen at discrete times "tj" (where j indexes all the times at which switching of a given MOSFET occur) and for a short period; they occur under the following circumstances (Mohanet al. n.d.):

- switching of power currents ("turning on and off currents in the presence of voltage")
- parasitic drain capacitance charge and discharge
- gate drive losses
- body diode reverse recovery

An estimate of their magnitude can be obtained as follows:

• If the MOSFET is turning on, and the current was not flowing through its body diode, then the switching loss can be estimated as being proportional to the product of the current that will start to flow through the MOSFET and the voltage across the MOSFET prior to switching, i.e.:

$$P_{Switching,j} \sim v(t_j^-)i_L(t_j^+)$$

(3.15)

• If the MOSFET is turning off, on the contrary, and the current will not be able to flow through its body diode, then the switching loss can be estimated as being proportional to the product of the current that was flowing through it and the voltage that will be applied to the MOSFET after, i.e.:

$$P_{Switching,j} \sim v(t_j^+)i_L(t_j^-)$$

(3.16)

On a side note, it can be noted that since these losses occur at switching times, the more switching there are, the higher the switching losses will be (if the same MOSFETs are used), i.e. switching losses grow proportionally to the switching frequency. Therefore, on one hand, switching frequency should not be chosen to be arbitrarily high. But on the other hand, switching frequency should not be chosen too low either because that would cause higher ripples on the output voltage.

3.3 PROPOSED CONVERTER TOPOLOGY

The proposed converter topology [19] used in this project is designed to deliver output voltages both higher as well as lower than (and even equal to) the input voltage; this is done to exploit different possible combinations of solar panels and batteries available in the market.

Figure 3.3.1, depicts the circuit topology employed. It can be split into two separated voltage conversion stages, the "buck"-leg and the "boost"-leg; the first stage (the "buck"-leg) consists of switches T1 and T2, while the second stage (the "boost"-leg) contains switches T3 and T4. The circuit is divided in these two legs because it turns out that for proper functionality of the circuit (i.e. in order to avoid a voltage source to be short-circuited) each of these two pairs of switches (i.e. for example T1 and T2) need to work in a complementary manner. For T1 and T2 to work in a complementary manner means that when switch T1 is conducting current (it is on), switch T2 must be off, and vice-versa.

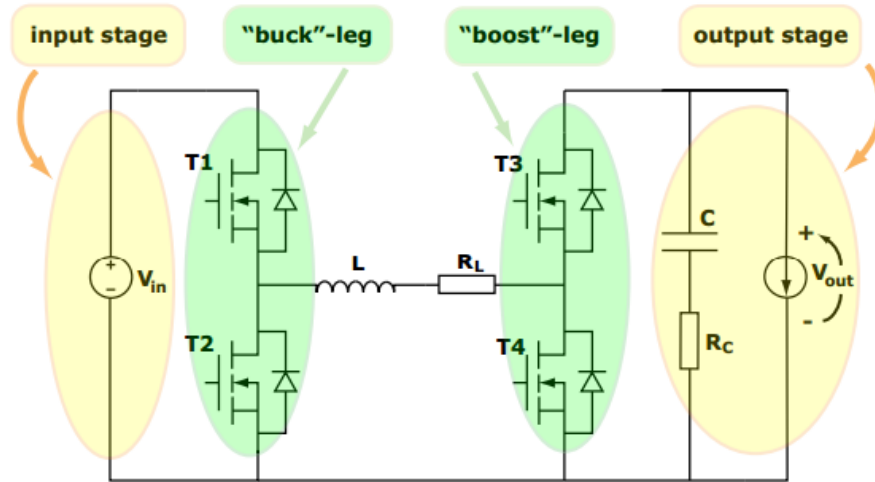Figure 3.3.1: Schematic of the circuit topology used to achieve DC-DC power conversion

Figure 3.3.2 shows a simplified diagram of how the four power switches are connected to the inductor, VIN, VOUT and ground. Figure 3.3.3 shows the regions of operation for as a function of VOUT −VIN.
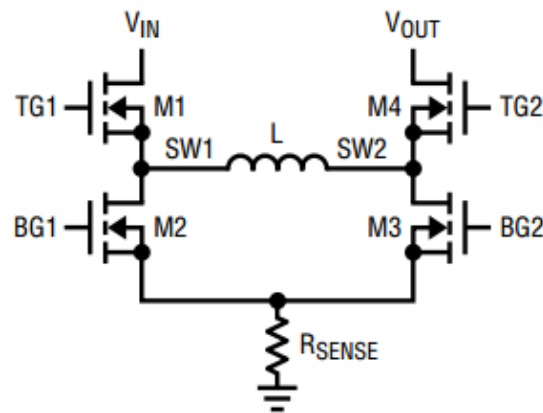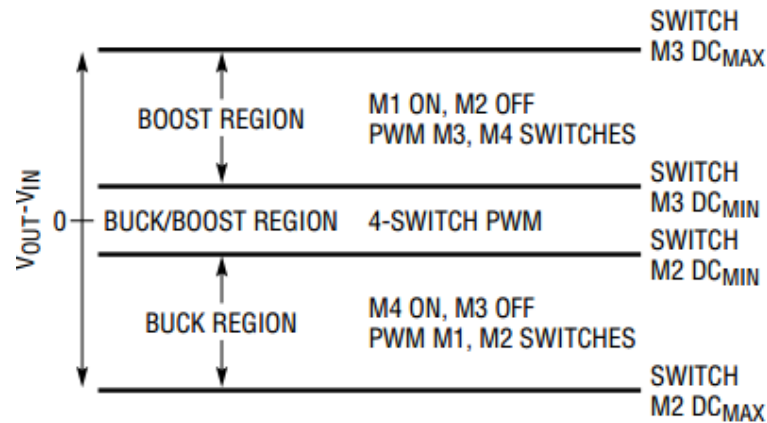

Figure 3.3.2: Simplified Diagram of the Output Switches [19]

Figure 3.3.3: Simplified Diagram of the Output Switches [19]

When VIN is significantly higher than VOUT, the converter will run in the **Buck** region. In this region switch M3 is always off. Also, switch M4 is always on unless reverse current is detected. At the start of every cycle, synchronous switch M2 is turned on first. After the sensed inductor current falls below the reference, switch M2 is turned off and switch M1 is turned on for the remainder of the cycle. Switches M1 and M2 will alternate (see Figure 3.3.4), behaving like a typical synchronous buck regulator.
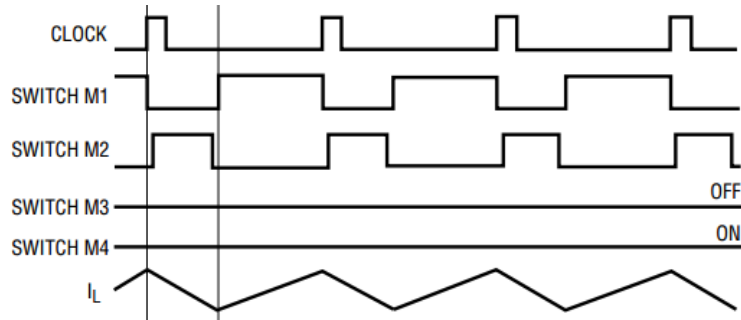

Figure 3.3.4: Switching Waveform, Buck Region (VIN >> VOUT) [19]

When VIN is close to VOUT, the controller enters the **Buck-Boost** region. Figure 3.3.5 shows typical waveforms in this region. Every cycle, if the controller starts with switches M2 and M4 turned on, the controller first operates as if in the buck region. Switch M2 is turned off and M1 is turned on until the middle of the clock cycle. Next, switch M4 turns off and M3 turns on. The controller then operates as if in boost mode. Finally switch M3 turns off and M4 turns on until the end of the cycle. If the controller starts with switches M1 and M3 turned on, the controller first operates as if in the boost region. Switch M3 is turned off and M4 is turned on until the middle of the clock cycle. Next, switch M1 turns off and M2 turns on. The controller then operates as if in buck mode. Finally switch M2 turns off and M1 turns on until the end of the cycle.
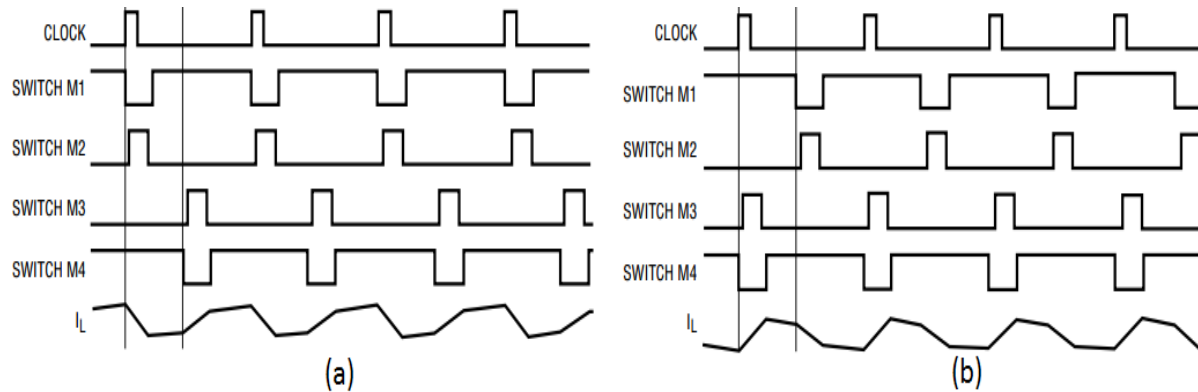

Figure 3.3.5: Switching Waveform (a) Buck-Boost Region (VIN ≥ VOUT), (b) Buck-Boost Region (VIN ≤ VOUT) [19]

32

When VOUT is significantly higher than VIN, the converter will run in the boost region. In this region switch M1 is always on and switch M2 is always off. At the start of every cycle, switch M3 is turned on first. Inductor current is sensed while switch M3 is on. After the sensed inductor current rises above the reference voltage, switch M3 is turned off and switch M4 is turned on for the remainder of the cycle. Switches M3 and M4 will alternate, behaving like a typical synchronous boost regulator.
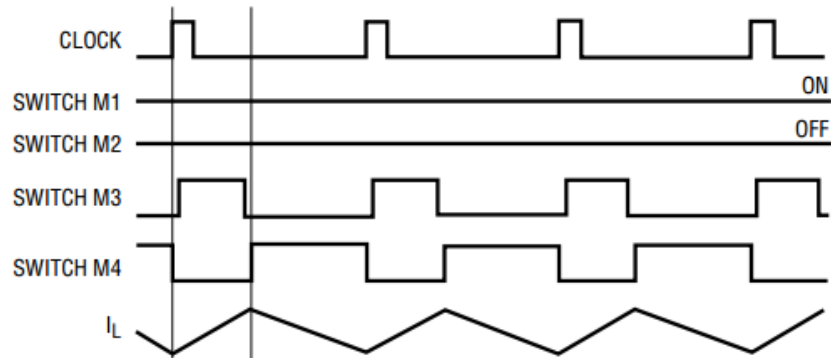

Figure 3.3.6: Switching Waveform, Boost Region (VIN << VOUT) [19]

3.4 DC/DC CONVERTER OPERATION IN SOLAR APPLICATIONS

Ideally, any system using a solar panel would operate that panel at its maximum power output. This is particularly true of solar powered lighting systems, where the goal, presumably, is to capture and store as much solar energy as possible in as little time as possible. Put another way, since we cannot predict the availability or intensity of solar power, we need to harness as much energy as possible while energy is available.

There are many different ways to try to operate a solar panel at its maximum power point. One of the simplest is to connect a battery to the solar panel through a diode. It relies on matching the maximum power output voltage of the panel to the relatively narrow voltage range of the battery; which is practically not possible to achieve in majority of the applications. The opposite end of the spectrum is an approach that implements a complete Maximum Power Point Tracking (MPPT) algorithm.

The MPPT algorithm proposed in Chapter 2 to perform this function. It finds the true maximum power operating point by periodically sweeping the entire output range of the solar panel and remembering the operating conditions where maximum power was achieved. When the sweep is complete, the DC/DC control converter circuitry forces the panel to return to its maximum power

point. In between these periodic sweeps, the MPPT algorithm will continuously dither the operating point of the DC/DC converter to ensure that it operates at the peak.

Battery charger with the solar lighting system maintains a solar panel at its peak operating efficiency by implementing input voltage regulation. When available solar power is inadequate to meet the power requirements (see Figure 3.4.1(a)), input voltage regulation reduces the battery charge current. This reduces the load on the solar panel to maintain the panel voltage at VMP, maximizing the panel output power. This method of achieving peak panel efficiency is called maximum power point control (MPPC).

The method works well for standalone solar lighting systems in warm and sunny locations, where sufficient solar power exists to top off the batteries however, in locations where overcast conditions limit the charging of the batteries through solar power, this becomes a challenge. The power conversion efficiency of the DC/DC converter within battery charger suffers when illumination (irradiation) levels are low as majority of the available power is lost in conduction and switching losses (see Figure 3.4.1(b)), degrading the overall power transfer efficiency from the panel to the battery.

The result is an inefficient transfer of charge to the battery, as the system is unable to deliver sufficient current needed for battery charging, hence stopping charge transfer at a higher level of sunlight than otherwise necessary.
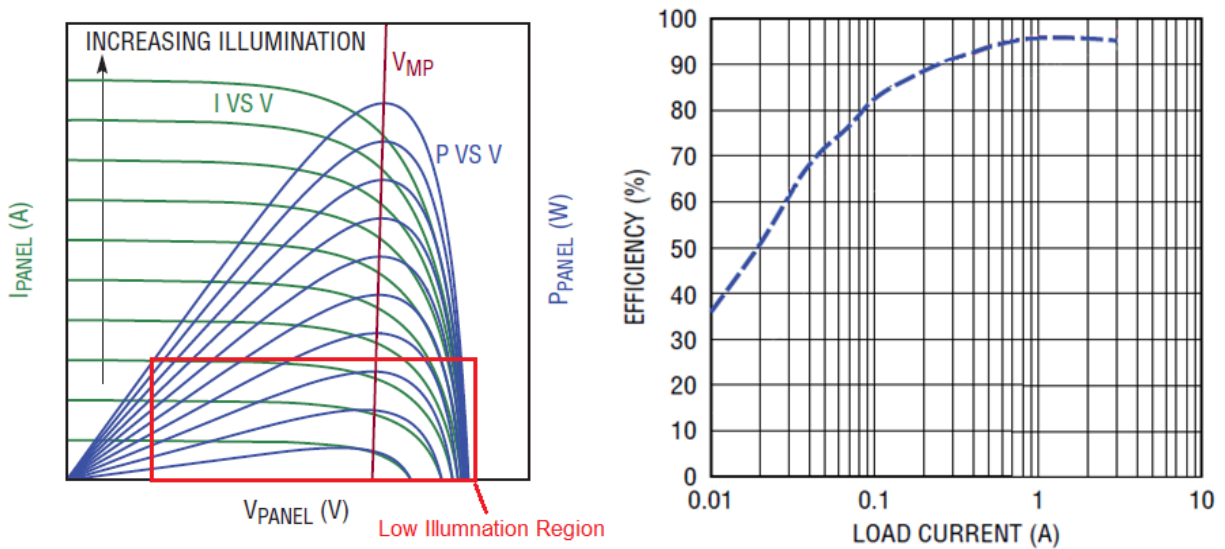

Figure 3.4.1: (a) Solar Panel IV curve under low illumination, (b) Power Conversion Efficiency under low input current conditions

3.5 PROPOSED SOLUTION TO MAINTAIN HIGHER EFFIENCY IN LOW LIGHT CONDITIONS (BURST CHARGING)

The proposed "Burst Charging" control technique presents a novel approach to the charging of the battery in low light levels (dusk) or during overcast days. When current from the solar panel is not high enough to reliably measure the maximum power point, the battery charger starts operating in "Burst" power mode. In this mode, the battery charger momentarily stops charging, allowing the panel voltage to rise. When the panel has sufficiently charged the input capacitor before the "buck stage" in proposed converter topology, battery charger then transfers energy from the input capacitor to the battery while drawing down the panel voltage. This behavior repeats rapidly, generating a charger output that is a series of high current bursts, which maximizes the efficiency as show in Figure 3.5.1 below.
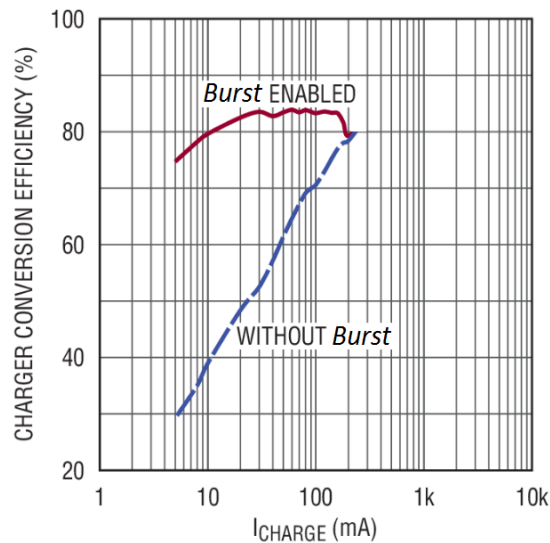
Figure 3.5.1: Power Conversion Efficiency with and without Burst Charging

- **Implementation and Verification**

In order to implement the proposed algorithm, a comparator is added to the current sensing circuitry within the battery charger. It is configured to trigger when the current output from the battery charger goes below a certain percentage of the programmed maximum current. During periods of low illumination, output current of the charger goes below this set point, causing the comparator output to become high. This pin change-of-state is used to disable the power stage by triggering an input under voltage lockout (UVLO) with the falling threshold at a solar panel voltage that is higher than V_{MP}. As solar panel voltage climbs through the UVLO hysteresis range in response to the power stage being disabled until the UVLO rising threshold is

achieved, the charger is then re-enabled at lower switching frequency which reduces switching losses even further delivering higher charge current until comparator again disables the charger. This cycle repeats as shown in Figure 3.5.2(b) below, generating a charger output that is a series of high current bursts. This maximizes the efficiency of the charger as well as the efficiency of the entire solar charger system at low illumination levels as depicted in Figure 3.4.1(a).

In order to verify the efficiency claim under "Burst" operation, an experiment was designed to collect data by operating the proposed converter under both normal and proposed algorithm. The results are presented in the Figure 3.5.2; which shows that under normal operation, the power converter in able to deliver 270 mA of current, whereas under burst operation the same system is able to deliver 610 mA. Burst charging increases overall charger efficiency up to about **2.5** times than that of during normal operation in low light conditions.

Figure 3.5.2: Delivered Power to the Battery; (a) under normal operation, (b) under proposed (Burst) operation

3.6 SUMMARY

In the first part of the chapter an overview of commonly used DC/DC converter topologies is presented, and their modes of operation are analyzed with the principle of inductor volt second balance. In the second part the converter topology used in this project is discussed. Furthermore, a new control technique, suitable for maintaining high power conversion efficiencies in low lighting conditions is proposed, and implementation details are given following the experimental results.

4. BATTERY SUBSYSTEM

Systems that utilize solar energy as its source require some sort of a storage device that stores the energy generated by the solar panels throughout the day, and use this stored energy when no sunlight is available. The most realistic type for this storage device is a backup battery. There are many different backup technologies available in the market today. In the following sections, the Lithium-Ion battery technology that has been selected for use in this project is discussed.

4.1 LITHIUM ION BATTERY

Lithium is one of the lightest metals, is one of the most reactive and has the highest electrochemical potential, making it the ideal material for a battery. A Li-ion battery contains no lithium in a metallic state, but instead uses lithium ions that shuttle back and forth between the cathode and anode of the battery during charge and discharge, respectively. The cathode is a metal oxide and the anode consists of porous carbon. Figure 4.1.1 illustrates the process.
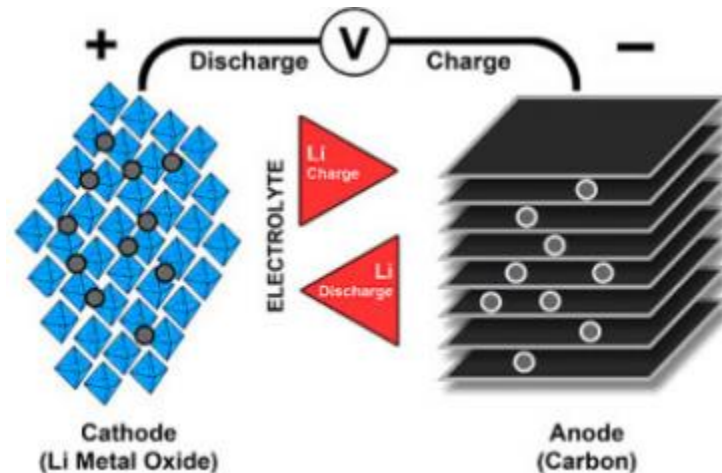

Figure 4.1.1: Ion flow in lithium-ion battery [20]

When the cell charges and discharges, ions shuttle between cathode (positive electrode) and anode (negative electrode). On discharge, the anode undergoes oxidation, or loss of electrons, and the cathode sees a reduction, or a gain of electrons. Charge reverses the movement.

Although there are many different types of Li-ion batteries, the most popular chemistries now in production can be narrowed down to three, all relating to their cathode materials. The advantages and disadvantages for each cathode material are summarized in the figure 4.1.2 below.

The battery selected for this project uses lithium-phosphate as the cathode material offers excellent safety and long life span which are essential qualities for off-grid solar applications.

Cathode materials	Advantages	Disadvantages
Lithium-cobalt-oxide (most common)	• High capacity	• Lower charge and discharge rates • Higher cost
Lithium-manganese-oxide	• Lower ESR • Higher charge and discharge rates • Higher temperature operation • Inherently safer	• Lower capacity • Lower cycle life • Shorter lifetime
Lithium-phosphate (newest)	• Very low ESR • Very high charge and discharge rates • High temperature operation • Inherently safer	• Lower discharge voltage • Lower float voltage • Lower capacity

Figure 4.1.2: Summary of different cathode materials in lithium-ion battery [20]

4.2 CYCLE LIFE & CAPACITY LOSS

All rechargeable batteries wear out, and Li-ion cells are no exception. Charging and discharging will eventually reduce the battery's active material and cause other chemistry changes, resulting in increased internal resistance and permanent capacity loss (see figure 4.2.1). Battery manufacturers usually consider the end of life for a battery to be when the battery capacity drops to 80% of the rated capacity and the number of full charge/discharge cycles after which the battery capacity drops to this limit is known as the cycle life of the battery.
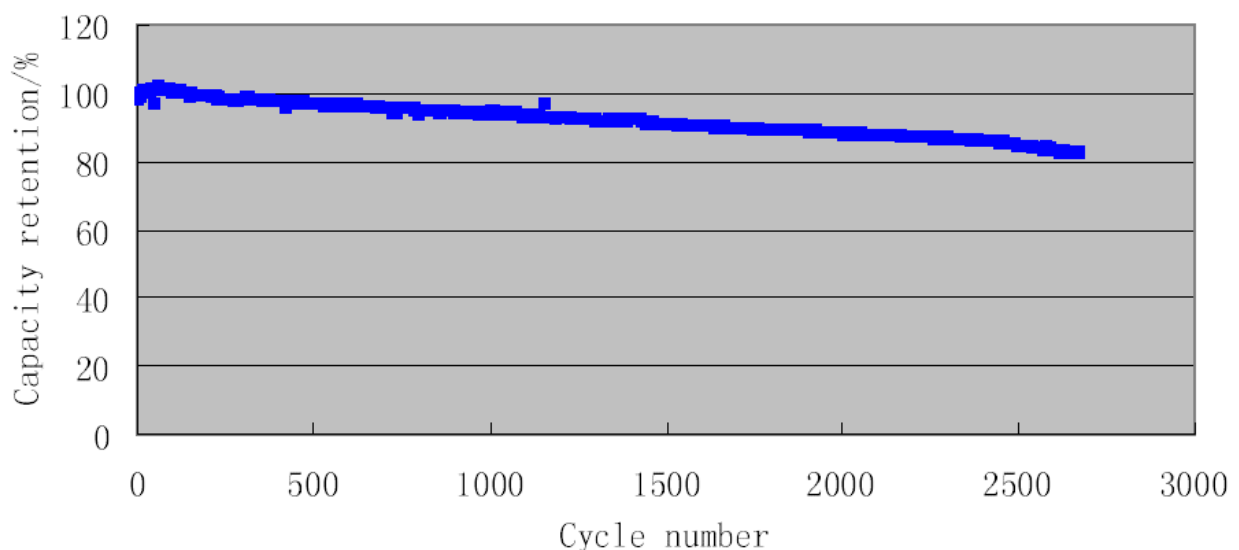

Figure 4.2.1: Capacity retention of a typical lithium phosphate battery over time

There are two types of battery capacity losses: recoverable loss and permanent loss. After a full charge, a Li-ion battery will typically lose about 5% capacity in the first 24 hours, then approximately 3% per month because of self-discharge and an additional 3% per month if the battery pack has pack-protection circuitry. These self-discharge losses occur when the battery remains around 20°C, but will increase considerably with higher temperature and also as the battery ages. This capacity loss can be recovered by recharging the battery.

Permanent capacity loss, as the name implies, refers to permanent loss that is not recoverable by charging. Permanent capacity loss is mainly due to the number of full charge/discharge cycles, battery voltage and temperature. Permanent capacity loss also occurs even when the battery is not in use and is greatest at elevated temperatures with the battery voltage maintained at full charge level. The more time the battery remains at 4.2 V or 100% charge level (or 3.6 V for Li-ion phosphate), the faster the capacity loss occurs. This is true whether the battery is being charged or just in a fully charged condition with the voltage near 4.2 V (3.6 for LFP). Always maintaining a Li-ion battery in a fully charged condition will shorten its lifetime. The chemical changes that shorten the battery lifetime begin when it is manufactured, and these changes are accelerated by high float voltage and high temperature (see Figure 4.2.2). Permanent capacity loss is unavoidable, but it can be held to a minimum and battery cycle life can be prolonged by observing good battery practices when charging, discharging or simply storing the battery. Using partial-discharge cycles can greatly increase cycle life, and charging to less than 100% capacity can increase battery life even further.
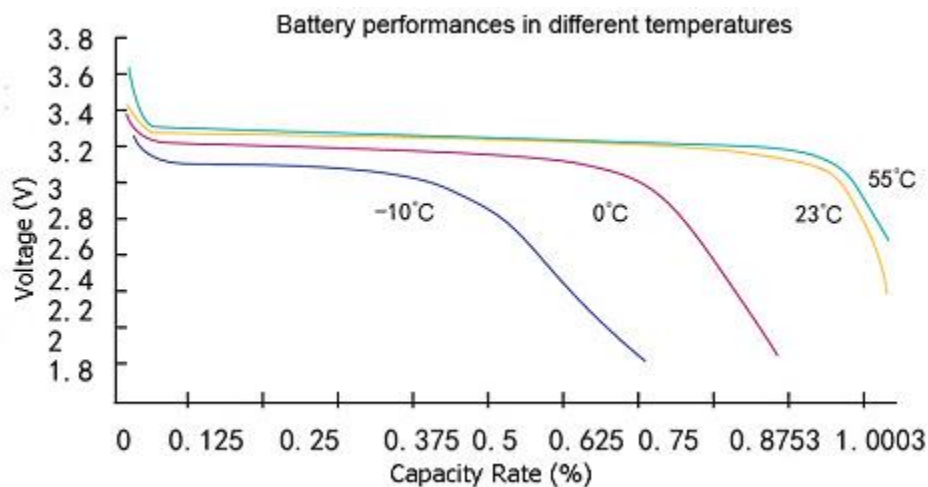

Figure 4.2.2: Battery performance in different temperatures

The letter "C" is a battery term used to indicate the battery manufacturers stated battery discharge capacity, measured in milliamp-hours. For example, a 2000-mAhr rated battery can supply a 2000-mA load for one hour before the cell voltage drops to its zero-capacity voltage. In the same example, charging the battery at a C/2 rate would mean charging at 1000 mA (1 A). C is important in battery chargers because it determines the correct charge current required and the length of time needed to fully charge a battery. When discussing minimum charge-current termination methods, a 2000-mAhr battery using C/10 termination would end the charge cycle when the charge current drops below 200 mA.

4.3 SAFETY CONCERNS IN LI-ION BATTERIES [21]

The performance and cycle of Lithium-ion cells is dependent on both the temperature and the operating voltage. The Figure 4.3 shows that, the cell operating voltage and temperature must be kept within the limits indicated by the green box at all times for the safe operation. Once outside the safety limits, permanent damage is inflicted to the cell.
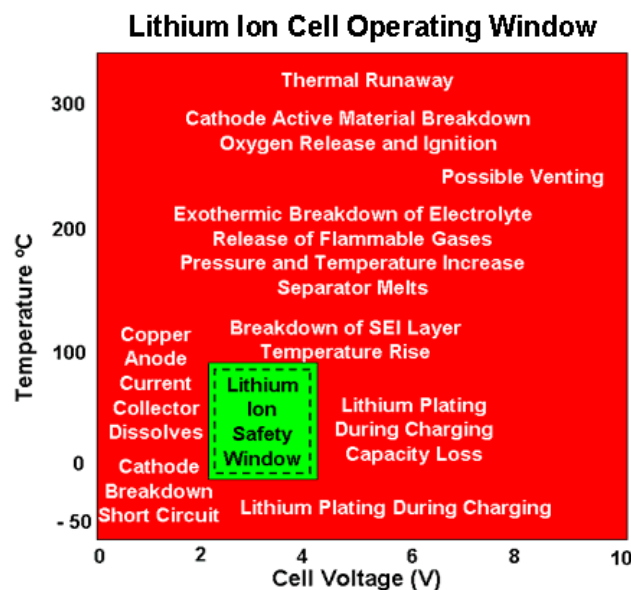

Figure 4.3: Li-Ion Cell Operating Window [21]

- **Voltage Effects**
  - *Over-Voltage*

    If the charging voltage is increased beyond the recommended upper cell voltage, excessive current flows can lead to two problems.

- Lithium Plating

    With excessive currents the Lithium ions cannot be accommodated quickly enough between the intercalation layers of the anode and start to accumulate on the surface of the anode where they are deposited as metallic Lithium. This is known as Lithium plating. This results in a reduction of freely available lithium ions causing an irreversible capacity loss.

  o *Under-voltage / Over-discharge*

    Allowing the cell voltage is allowed to fall below 2 Volts by over-discharging over extended period results in progressive breakdown of the electrode materials causing an irreversible loss in capacity.

- **Temperature Effects**

  o *Low temperature operation*

    The rate at which chemical reaction occurs is reduced in line with temperature (Arrhenius Law). Since the charge is stored in the battery as a result of chemical activity, reducing the temperature limits current carrying capacity of the cell both for charging and discharging. Furthermore, at low temperatures, the reduced reaction rate slows down, and makes the insertion of the Lithium ions into the intercalation spaces more difficult. As with over-voltage operation, when the electrodes cannot accommodate the current flow, the result is reduced power and Lithium plating of the anode with irreversible capacity loss.

  o *High temperature operation*

    Operating at high temperatures brings higher power out of the cell by increasing the reaction rate. Higher currents will also give rise to higher I^2R heat dissipation increasing the temperature even higher starting positive temperature feedback and unless heat is removed faster than it is generated the result will be thermal runaway bursting battery into flames.

For increased capacity, Li-ion cells are often connected in parallel. No special requirements are needed, other than the batteries should be the same chemistry, manufacturer and size. Series-connected cells require more care because cell-capacity matching and cell-balancing circuitry are often required to assure that each cell reaches the same float voltage and the same level of charge

to avoid any excessive discharge from one cell to the other.

4.4 LI-ION CHARGING METHODS

The recommended way to charge a Li-ion battery is to provide a ±1% voltage-limited constant current to the battery until it becomes fully charged, and then stop. Methods used to determine when the battery is fully charged include timing the total charge time, monitoring the charge current or a combination of the two. The first method applies a voltage-limited constant current, ranging from C/2 to 1C for 2.5 to 3 hours, thus bringing the battery up to 100% charge. You also can use a lower-charge current, but it will require more time. The second method is similar, but it requires monitoring the charge current. As the battery charges, the voltage rises, exactly as in the first method. When it reaches the programmed voltage limit, which is also called the float voltage, the charge current begins to drop. When it first begins to drop, the battery is about 50% to 60% charged. The float voltage continues to be applied until the charge current drops to a sufficiently low level (C/10 to C/20), at which time the battery is approximately 92% to 99% charged and the charge cycle ends. This scheme of charging is called Constant Current-Constant Voltage (CC-CV). Fig. 4.4 shows a typical Li-ion charge profile's charge current, battery voltage and battery capacity versus time.
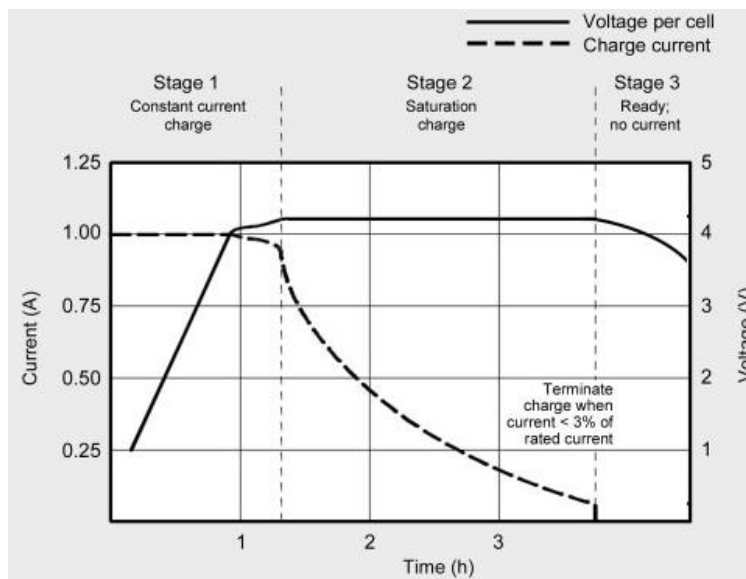

Figure 4.4: The constant-current, constant-voltage charge profile for a Li-ion battery depends on the charge current, cell voltage and charge capacity [20]

Applying a continuous voltage to a battery after it is fully charged is not recommended, as it will accelerate permanent capacity loss and may cause internal lithium metal plating. This plating can

develop into an internal short circuit, resulting in overheating and making the battery thermally unstable.

Most of the Li-Ion battery chargers available in the market do not offer lower float-voltage option through which the battery life can be increased.

4.5 PROPOSED CHARGING METHOD

Battery charger's role in extending battery lifetime is mainly determined by the charger's float voltage and charge termination method. A flexible charging method is proposed that offers flexibility in both the programmable float-voltage and charge-current termination method. It can provide a longer battery life by selecting the correct level at which to end the charge cycle. The charging method also employs battery temperature sensing whose main purpose is to prevent charging if the battery temperature is outside the recommended window of 0°C to 50°C. The charging profile shown in Figure 4.5.1, is composed of 3 stages. Description for each stage is given in Table 4.1.

Stage 0, heavily discharged battery is preconditioned with configurable reduced constant current. The stage occurs for battery voltages between 35% - 70% of the Stage 2 voltage limit.

Stage 1, battery is charged with configurable constant current equal to or higher than in Stage 0. This constant current stage occurs for battery voltages between 70% - 98% of the Stage 2 voltage limit.

Stage 2, battery is supplied with configurable constant voltage. This constant voltage stage occurs for battery voltages above 98% of the Stage 2 voltage limit.
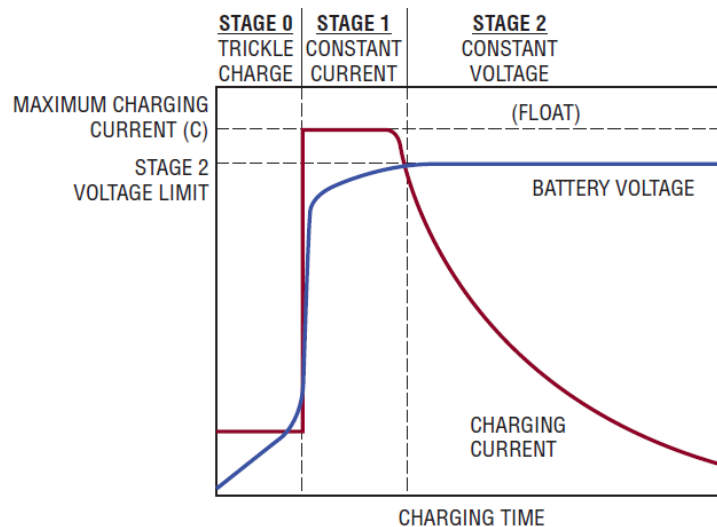

Figure 4.5.1: Proposed constant-current, constant-voltage charge profile

STAGE	NAME	METHOD	DURATION
0	Trickle Charge	Constant Current at a Configured Fraction of Full Charge Current	Until Battery Voltage Rises Above V_{S0} (70% of Stage 2 Voltage Limit)
1	Constant Current	Constant Full Charge Current	Until Battery Voltage Rises Above V_{S1} (98% of Stage 2 Voltage Limit)
2	Constant Voltage	Constant Voltage	Until Charging Current Falls Below C/10 or Optional Timed Charging

Table 4.1: Description of charging stages

4.6 RUN-TIME VERSUS BATTERY LIFE

With present battery technology and without increasing battery size, you can't get both longer run-time and longer battery life. For maximum run-time, the charger must charge the battery to 100% capacity. This places the battery voltage near the manufacturer's recommended float voltage. Unfortunately, charging and maintaining the battery near these levels shortens battery life. One solution is to select a lower float voltage, which prohibits the battery from achieving 100% charge, although this would require a higher-capacity battery to provide the same run-time. Also, using a C/10 minimum charge-current termination method can have the same effect on battery life as using a lower float voltage. Reducing the float voltage by 100 mV will reduce capacity by approximately 15%, but can double the battery cycle life [20].

4.7 PROPOSED RUN-TIME EXTENSION ALGORITHM FOR SOLAR LIGHTING APPLICATION

In this section an algorithm is proposed that maximizes battery run-time in off-grid solar lighting application. It predicts the upcoming number of overcast days during which the charge delivered to the battery is minimum through a weather forecast. The "cloud cover" data within the weather forecast is translated into the amount of charge expected and light dimming profile is then adjusted so that the system is able to survive during the programmed number of dark days.

The calculations for the allowed light level are made using the equations presented below;

$$\text{Remain\_Cap} = ((\text{Cur\_SoC}) / 100 * \text{Full\_Cap}) - \text{Low\_Lvl\_Cutoff} \qquad \text{(a)}$$

$$\text{Max\_Dis\_Current} = (1/\text{No\_Dark\_Days} * \text{Remain\_Cap} + \text{Exp\_Chrg}) / \text{Night\_Length} \qquad \text{(b)}$$

Where;

Remain_Cap = Remaining capacity available for discharge

Cur_SoC = Current State-of-Charge of the battery

Full_Cap = Full charge capacity of the battery

Low_Lvl_Cutoff = Low level disconnect threshold where the battery is disconnected.

Max_Dis_Current = Maximum amount of discharge current allowed during the night

No_Dark_Days = Number of dark days the system is programmed to sustain

Exp_Chrg = Expected charge derived from the cloud cover data

Night_Length = Number of hours during the night the light will be turned ON.

Let us consider a weather scenario presented in Figure 4.7.1; during the first two days, enough sunlight is available to completely charge the battery whereas the next 5 days are overcast and no charge is expected to be transferred to the battery. Let us assume, the system based on a 10Ah battery, and the LED luminaire consumes 240mA at full light intensity. It is programmed to survive 5 dark days. Note the battery float voltage is lowered to 92% to extend battery life and a cut-off voltage threshold is set at 20%. This leaves with an available discharge capacity after a complete charge of around 72%.

The system is simulated under this weather scenario with and without the proposed run-time extension algorithm and the results are visualized in Figure 4.7.2.

After the first 2 bright days, the RTE calculation will be triggered before turning ON the light on the third day. Let us assume the night length is 8 hours;

Remain_Cap = (0.92 * 10) − 2 = 7.2 Ah

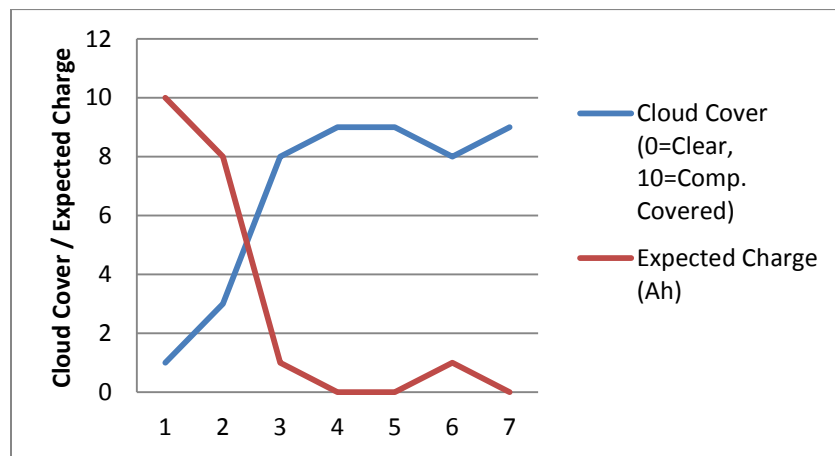Max_Dis_Current = (0.2 * 7.2 + 0) / 8 = 180mA ~= 70% Light Profile

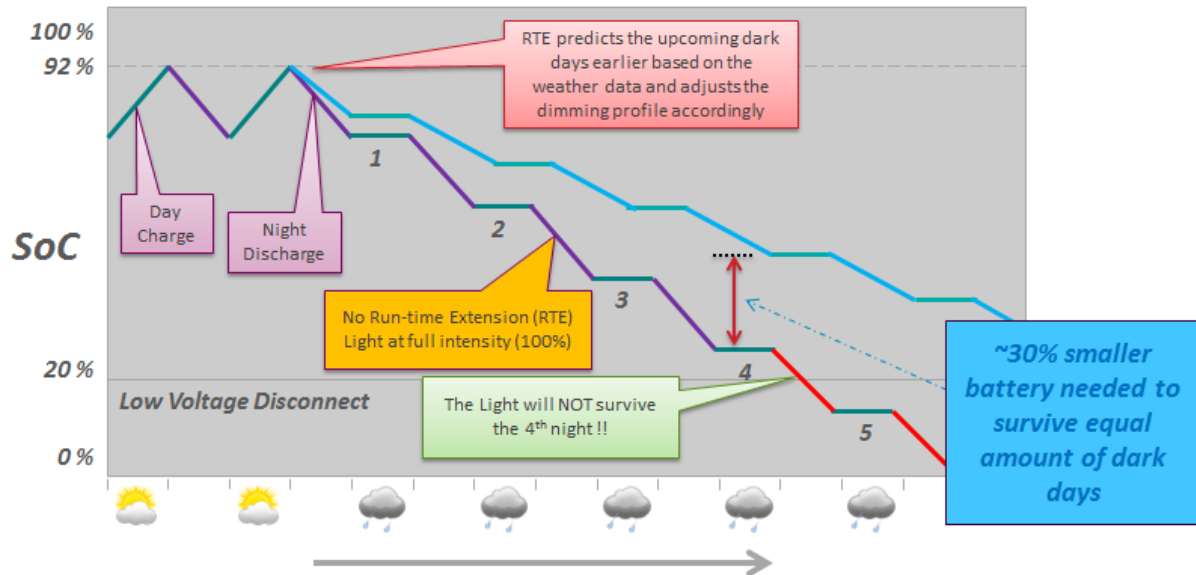Table 4.7.1: Cloud Cover and Expected Charge data for 7 days

Table 4.7.2: Simulation Results with and without Run-Time extension

As can be seen from the simulation results that with proposed Run-Time Extension algorithm, the system will be able to survive 5 consecutive darks days whereas without RTE the light will stay at 100% intensity and the system will shut down after 4 days. The results also suggest that a system with RTE will be able to survive the equal number of dark days as non-RTE with 30% smaller battery.

4.8 SUMMARY

In the first part of the chapter an overview of the Lithium-ion battery technology and related security concerns is presented. In the second part Li-ion charging methods are discussed and a flexible approach in proposed. Furthermore, a new run-time extension algorithm is proposed that adopts the load profile based of the weather data to maximize run-time.

5. EXPERIMENTAL RESULTS

5.1 PROTOTYPE CHARGE CONTROLLER

A prototype charge controller is constructed with several evaluation boards and developments kits to test and evaluate and functionality of the proposed maximum power tracking, low light burst charging and run-time extension algorithms proposed in the preceding chapters of this report. The algorithms are implemented on a low power ARM Cortex M3 microcontroller STM32L152.

Prototype charge controller is based on Linear Technology's LTC4020 battery charger demo board. It features the same 4 switch synchronous buck-boost topology discussed in Section 3.3. LTC4020 chip features input/output voltage regulations loops that offer the possibility to change input and output voltages dynamically while the converter is operating. This characteristic is used in the prototype charge controller to implement MPP tracking by inducing an external voltage signal through the microcontroller in the input regulation feedback path. The dedicated shutdown pin is also used in the similar manner by the microcontroller to implement burst charging scheme as described previous in Section 3.5. Constant-current/constant-voltage (CC/CV) battery charging state machine with either C/10 or timed termination described in Section 4.5 is also embedded in prototype charge controller. Simplified schematics of the LTC4020 demo board used in the prototype charger design is shown in figure 5.1.1. More information on this can be found in [19].
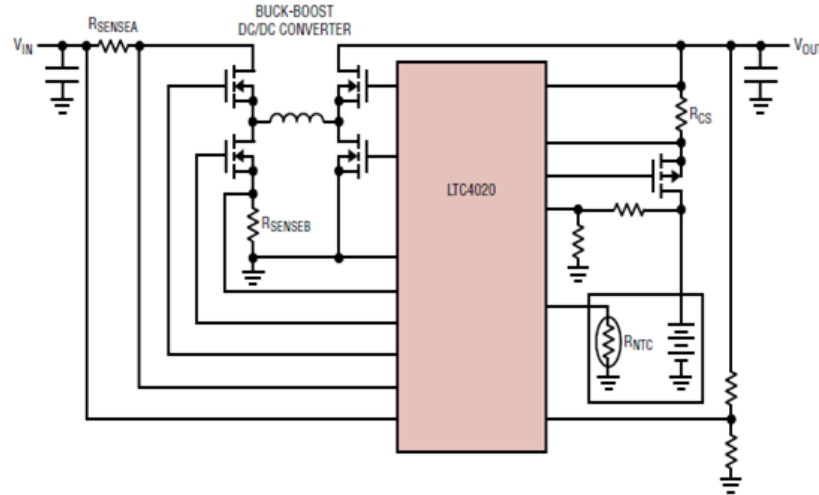

Figure 5.1.1 Simplified schematics of the LTC4020 demo board [19]

The output voltage of LTC4020 demo board is set to 28.80V to match the floating voltage of the 8S4P Lithium-phosphate battery pack used in the experiments and CC/CV charging with C/10

charge termination is enabled. This would change the respective Stage 0,1 voltage limits of the charge cycle to 20.16V and 28.23V respectively.

Two Yingli 120W solar panels connected in series are used for testing. In this arrangement the maximum power point of the panels is at 35V. The threshold for burst charging is set according to 25V in the software it only triggers in low illumination levels.

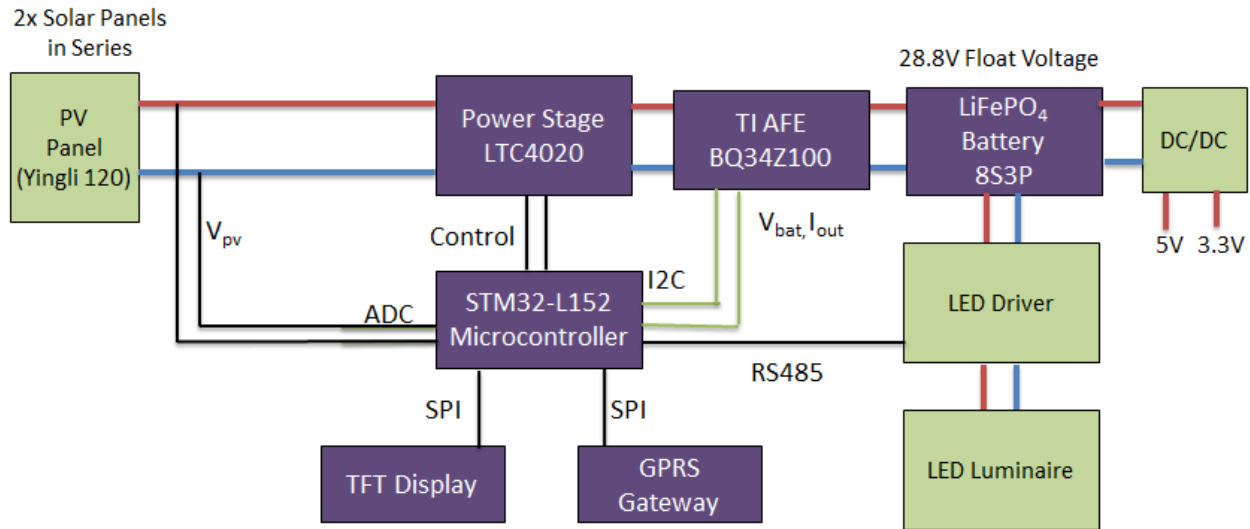System level overview of the prototype charge controller is shown in figure 5.1.2 below.

Figure 5.1.2: System Level Overview of Prototype Charge Controller

The output of the solar panel is connected to input of the prototype controller, the output from the power stage is routed through a shunt in Texas Instruments BQ34Z100 fuel gauge to the battery. The fuel gauge is used to continuous monitor the state-of-charge of the battery. PV panel voltage sensed directly though the ADC on the microcontroller. Battery voltage and current is sensed continuously by the fuel gauge, which sends this information to the microcontroller over the I2C bus. Dimming commands are sent to LED driver over RS485. TFT module is used to display the sensed parameters in on the screen. Microcontroller periodically sends the sensed data through the GPRS gateway to a cloud platform, where it is logged and can be viewed remotely. Designed prototype charge controller is shown in Figure 5.1.3.

5.2 EXPERIMENTAL RESULTS

The developed prototype charge controller was deployed for testing in one of demo solar poles at High Tech Campus in Eindhoven, Netherlands (see Figure 5.2.1). The experimental data collected over one day period is shown in Figure 5.2.2
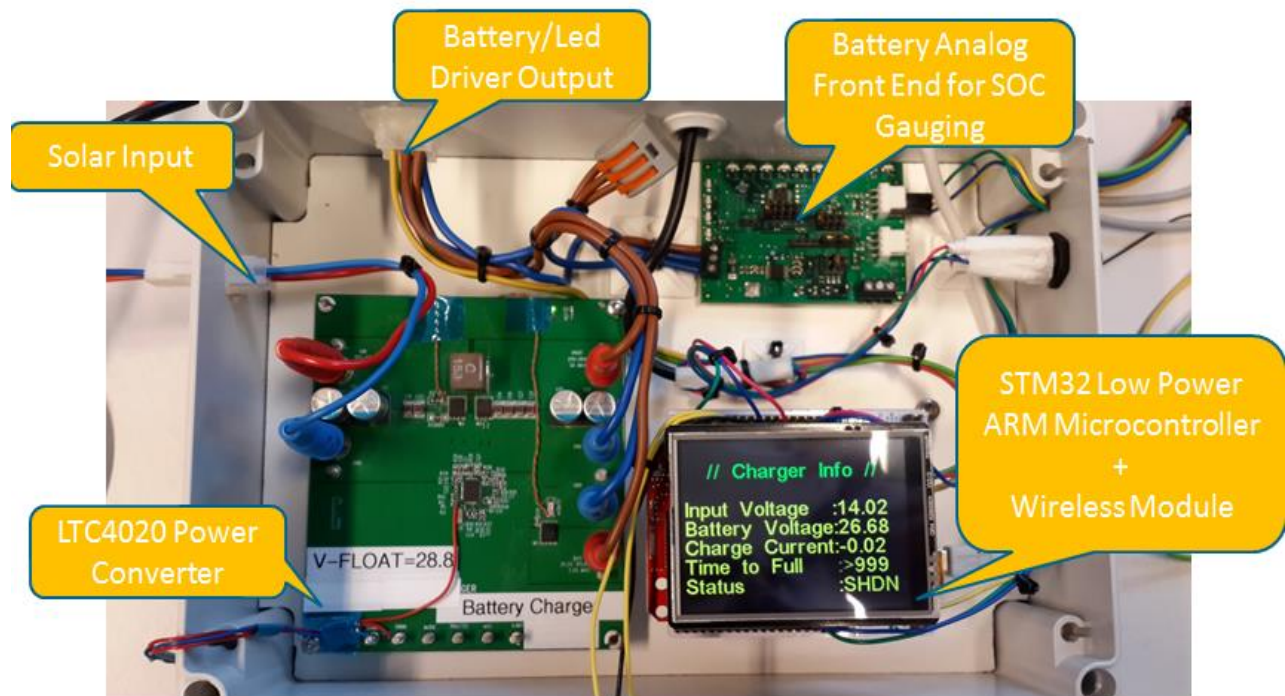
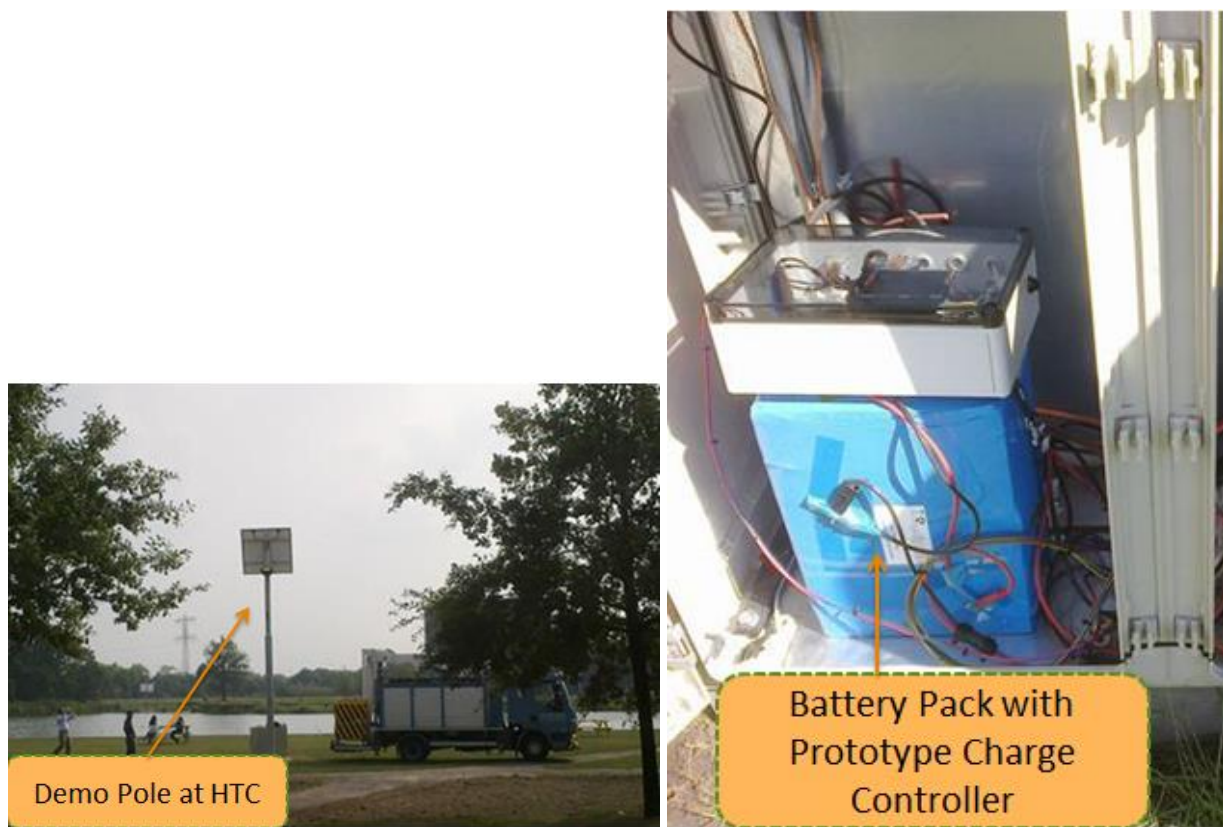Figure 5.1.3 Prototype Charge Controller

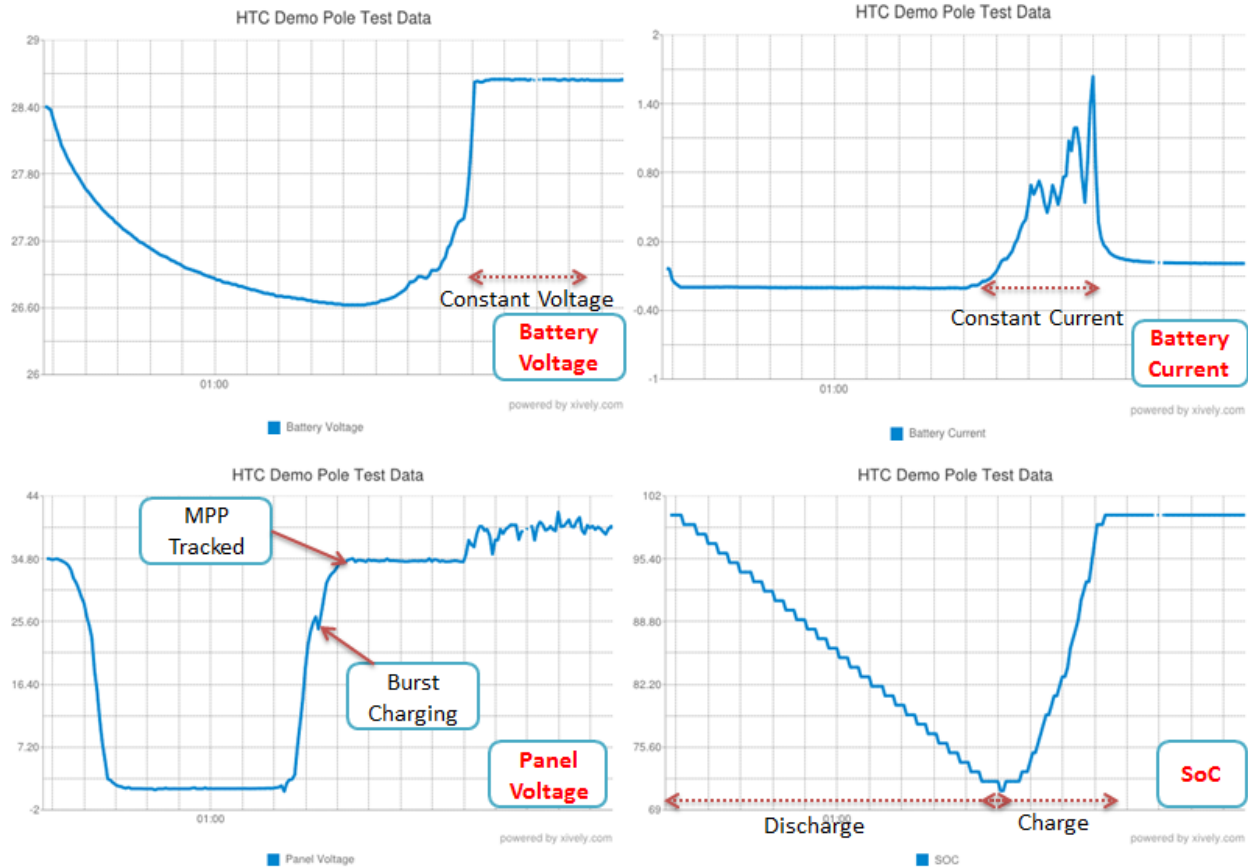Figure 5.2.1 Prototype charge controller deployment at HTC test poles

Figure 5.2.2 Prototype controller's experimental data over one day period

In order to verify the functionality of maximum power tracking burst charging mechanism, the battery is discharged during the night by turning ON the LED luminaire. Just before dawn, the luminaire is turned OFF and the battery is allowed to charge. We can see from the figure that as the voltage of the panel starts to rise, burst charging kicks in at the pre-defined threshold of 25V. It stays in this mode until the panel is able to deliver sufficient charging current. The charger stays in constant current stage and battery voltage starts rising as charge is being delivered to it. On the other hand maximum power tracking algorithm is able to accurately track the maximum power point as the panel voltage is kept in the close vicinity of 35V threshold. As soon as the battery voltage reaches the Stage 1 threshold, the charge cycle is switched from constant-current (CC) to constant-voltage (CV) and the battery voltage is kept at the float level till the rest of the period. At this stage the MPP tracking is disabled since there is no significant load demand and the power delivered by floating the panel voltage is sufficient to keep the charger in CV. The results presented in figure 5.2.2 therefore, validate that the maximum power tracking and burst charging algorithms are working properly as intended.

A similar experimental data over a period of 13 days is presented in figure 5.2.3.
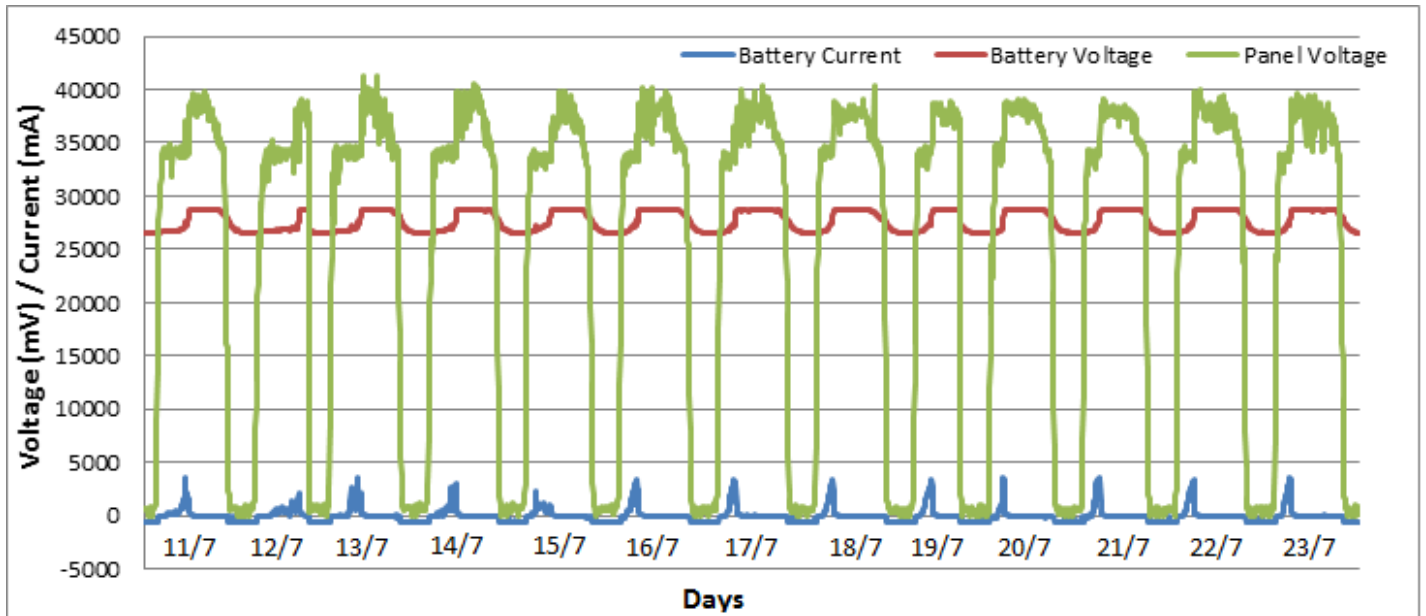

Figure 5.2.3 Prototype controller's experimental data over 13 days period
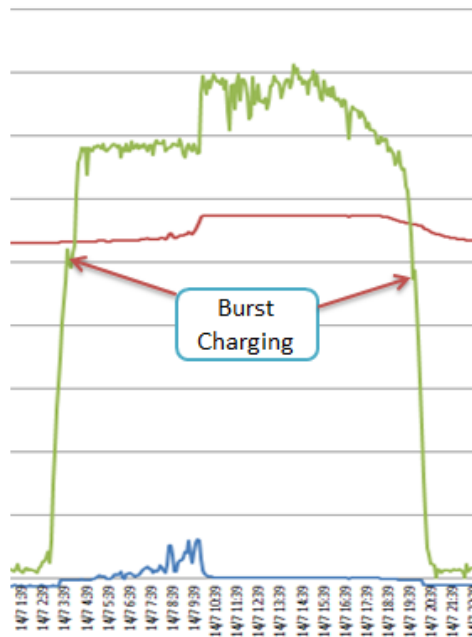
Figure 5.2.4 Enlarged section from experimental data over 13 days period

If we carefully analyze the results presented in figure 5.2.3, we can clearly see that there were some days during which the battery reached its float voltage fairly quick compared to the others; this implies there were some good days with sufficient sunlight and some bad ones. Day2 (12/7) is an example of a bad one; it took the battery charger long time to top off the battery to its full

capacity.

Based on the results, it's clear that irrespective of the weather condition, the prototype charge controller performed reliably; it was able to track the maximum power point with higher accuracy and less steady state oscillations. Figure 5.2.4 confirms that burst charging was triggered correctly at the right threshold; both early in morning and late in the evening as intended.

The dimming profile for LED luminaire was kept same during the experiment, so the battery starts its charge cycle the next morning at the similar voltage level. This is done with two things in mind; (a) make comparison easier, (b) use the value of time it takes to completely recharge the battery to calculate how much charge can be expected on a particular day. This information is then be correlated with weather prediction data (see Figure 5.2.5) to calibrate run-time extension algorithm by creating a table that related the cloud cover index to battery charge expected.
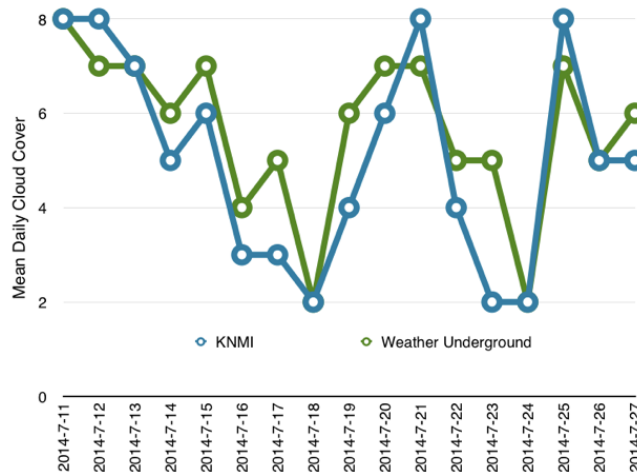

Figure 5.2.5 Weather prediction data

Figure 5.2.6 shows LED dimming profile of prototype charge controller with run-time extension after calibration.
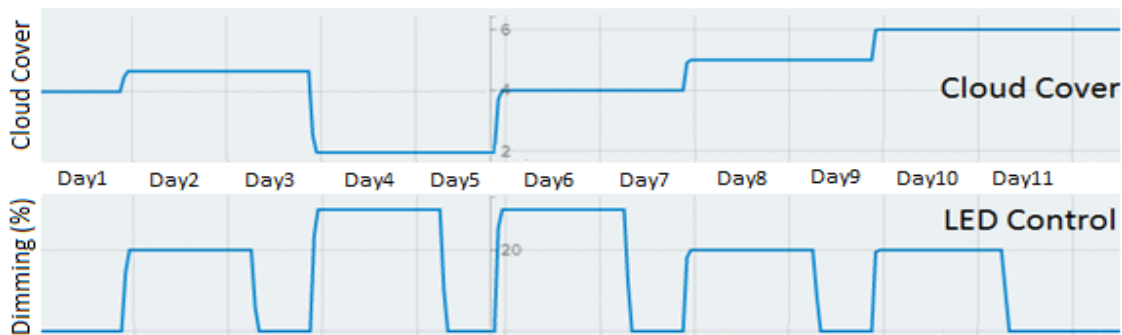
Figure 5.2.6 LED dimming profile with RTE

It can be clearly seen that RTE is able to properly predict an overcast day in advance and take appropriate action in time. For example, weather is moderately overcast on Day 2 and 3. RTE reduces the light profile to conserve charge in order to allow the system to survive for a longer time. On Day 3 evening before turning ON the light, RTE predicts that the upcoming day is going to sunnier so it increases the light profile. Opposite action is taken on Day 7 evening and light profile is reduced because RTE predicts that upcoming days are going to be overcast and charge need to be preserve to maximize run-time.

6. Conclusions

6.1 SUMMARY

Despite their benefits of clean and non-polluting energy generation, solar-powered lighting systems are still considered to be expensive and new algorithms that result in cost reduction of such systems is subject to extensive research.

In this work, new algorithms are proposed that aim at maximizing the energy output of a given PV panel, increase power conversion efficiency in low light conditions and prolonging cycle life of the rechargeable battery.

Chapter 2 begins with introduction to PV panels and their electrical characteristics. Starting from these characteristics, the importance of maximum power point tracking (MPPT) units has been shown. This was followed by addressing the common issues that most MPPT algorithms suffer from. Both of the most popular MPP trackers, the P&O and the INC share the shortcoming of possible misdirectional tracking during rapidly changing conditions due to their inability to distinguish the result of their own perturbations from the environmental changes. A new algorithm has been proposed to overcome this drawback. It incorporates new schemes for overcoming the challenges with associated with rapidly changing irradiation levels and the effect of partial shading.

Chapter 3 begins with an overview of the commonly used DC/DC converter topologies. The operations of these common topologies are analyzed with the principle of inductor volt second balance. Following that the converter topology used in this project is discussed. Furthermore, a new control technique, suitable for maintaining high power conversion efficiencies in low lighting conditions is proposed, and its implementation details are presented. Finally experimental results are presented to validate the claim.

Chapter 4 begins with an overview of the Lithium-ion battery technology and its related security concerns. Different Li-ion charging methods are discussed and a flexible charging approach in proposed. Following that, a run-time extension algorithm is presented that adopts the light profile based of the weather data to maximize system run-time.

Chapter 5 begins with a brief introduction to the implementation details of the prototype charge controller. This is followed by the experimental results that are analyzed to validate the benefits offered by the proposed algorithms.

6.2 FUTURE WORK

The attempts made in this thesis to contribute to the improvement in MPP tracking, burst charging in low light conditions and run-time extension have far from finished the task in these subjects. There is a lot of room for improvement, especially in run-time extension, which is a relatively new area.

Regarding MPPT control, it would be interesting to investigate the possibility of extending the tracking functionality to "burst" operation of the power converter. Currently the proposed algorithm periodically sweeps the entire I-V characteristic of the solar panel to detect partial shading which results in energy losses and an optimization of this process could be an interesting research topic.

For burst charging, it would be interesting to investigate the prolonged effects of continuous high current pulses on the cycle life performance of the battery and if it can be used to properly condition Li-ion batteries in low temperatures (reduce lithium plating).

It would also be nice to expand the concept of run-time extension to charging process, so parameters like float-voltage, battery current and charge termination method can be adjusted dynamically to create a flexible charge schedule which takes weather prediction data into account to maximizes run-time while prioritizing prolonging of cycle life.

7. REFERENCES

[1]   Fthenakis, Vasilis, James E. Mason, and Ken Zweibel. "The Technical, Geographical, and Economic Feasibility for Solar Energy to Supply the Energy Needs of the US" Energy Policy, Elsevier 32.2 (2009): 387-99. doi: 10.1016/j.enpol.2008.08.011.

[2]   The European Union climate and energy package, (The "20 – 20 – 20" package), http://ec.europa.eu/clima/policies/eu/package_en.htm.

[3]   Lighting Africa (n.d.). Solar Lighting for the Base of the Pyramid, Retrieved from http://www.ifc.org/wps/wcm/connect/a68a120048fd175eb8dcbc849537832d/SolarLightingBasePyramid.pdf?MOD=AJPERES.

[4]   H.L. Tsai, C.S. Tu, and Y.J. Su. Development of Generalized Photovoltaic Model Using MATLAB/SIMULINK. 2008.

[5]   Ortiz-Conde, F.J. Garc´ıa S´anchez, and J. Muci. New method to extract the model parameters of solar cells from the explicit analytic solutions of their illuminated I–V characteristics. Solar Energy Materials and Solar Cells, 90(3):352–361, 2006.

[6]   T. Markvart, Solar electricity, Wiley, 2000, p. 280.

[7]   D. Hohm and M. Ropp, "Comparative study of maximum power point tracking algorithms using an experimental, programmable, maximum power point tracking test," in Photovoltaic Specialists Conference, 2000. Conference Record of the Twenty-Eighth IEEE, 2000, pp. 1699–1702.

[8]   C. Hua, J. Lin, and C. Shen, "Implementation of a dsp-controlled photovoltaic system with peak power tracking," Industrial Electronics, IEEE Transactions on, vol. 45, no. 1, pp. 99–107, 1998.

[9]   "Perturb and Observe MPPT technique robustness improved," in Industrial Electronics, 2004 IEEE International Symposium on, vol. 2, 2004, pp. 845–850 vol. 2.

[10]   K. Hussein, I. Muta, T. Hoshino, and M. Osakada, "Maximum photovoltaic power tracking: an algorithm for rapidly changing atmospheric conditions," Generation, Transmission and Distribution, IEE Proceedings-, vol. 142, no. 1, pp. 59–64, 1995.

[11]   N. Femia, G. Petrone, G. Spagnuolo, and M. Vitelli, "Optimizing sampling rate of P&O MPPT technique," in Power Electronics Specialists Conference, 2004. PESC 04. 2004 IEEE 35th Annual, vol. 3, 2004, pp. 1945–1949 Vol.3.

[12]   C. Dorofte, U. Borup, and F. Blaabjerg, "A combined two-method mppt control scheme for grid-connected photovoltaic systems," in Power Electronics and Applications, 2005 European Conference on, 2005, pp. 10 pp.

[13]   B. Bletterie, R. Bruendlinger, and S. Spielauer, "Quantifying dynamic MPPT performance under realistic conditions First test results U the way forward," in ˝ 21st European Photovoltaic Solar Energy Conference and Exhibition, September 2006.

[14]   C. W. Tan, T. C. Green, and C. A. Hernandez-Aramburo, "Analysis of Perturb and Observe Maximum Power Point Tracking Algorithm for Photovoltaic Applications," presented at the 2nd IEEE International Conference on Power and Energy, Johor Baharu, Malaysia, Dec 2008.

[15]   Mäki, Anssi. "Effects of Partial Shading Conditions on Maximum Power Points and Mismatch Losses in Silicon-Based Photovoltaic Power Generators."Tampereen teknillinen yliopisto. Julkaisu-Tampere University of Technology. Publication; 1157 (2013).

[16]   Ovaska, Seppo. Maximum Power Point Tracking Algorithms for Photovoltaic Applications. Diss. Aalto University, 2010.

[17]   Vujanic, Robin. "Design and Control of a Buck-Boost DC-DC Power Converter." (2008).

[18]   Robert W Erickson, Fundamentals of Power Electronics, International Thomson Publishing (1997).

[19]   Linear Technologies, LTC4020 - 55V Buck-Boost Multi-Chemistry Battery Charger, Retrieved from http://www.linear.com/product/LTC4020.

[20]   Battery University, Lithium-Ion Batteries, Retrieved from http://batteryuniversity.com/learn/article/lithium_based_batteries.

[21]   Lithium Battery Failures, Retrieved from http://www.mpoweruk.com/lithium_failures.htm.